The Astrophysical Journal, 749:43 (17pp), 2012 April 10 doi:10.1088/0004-637X/749/1/43

KINEMATICS AND EXCITATION OF THE RAM PRESSURE STRIPPED IONIZED GAS FILAMENTS IN THE COMA CLUSTER OF GALAXIES*

Michitoshi Yoshida[1], Masafumi Yagi[2], Yutaka Komiyama[2], Hisanori Furusawa[3], Nobunari Kashikawa[2], Takashi Hattori[4], and Sadanori Okamura[5]
[1] Hiroshima Astrophysical Science Center, Hiroshima University, Higashi-Hiroshima, Hiroshima 739-8526, Japan; yoshidam@hiroshima-u.ac.jp
[2] Optical and Infrared Astronomy Division, National Astronomical Observatory, Mitaka, Tokyo 181-8588, Japan
[3] Astronomical Data Center, National Astronomical Observatory of Japan, Mitaka, Tokyo 181-8588, Japan
[4] Subaru Telescope, National Astronomical Observatory of Japan, 650 North A'Ohoku Place, Hilo, HI 96720, USA
[5] Department of Astronomy, University of Tokyo, Tokyo 113-0033, Japan
Received 2011 October 23; accepted 2012 February 2; published 2012 March 20

ABSTRACT

We present the results of deep imaging and spectroscopic observations of very extended ionized gas (EIG) around four member galaxies of the Coma Cluster of galaxies: RB 199, IC 4040, GMP 2923, and GMP 3071. The EIGs were serendipitously found in an Hα narrowband imaging survey of the central region of the Coma Cluster. The relative radial velocities of the EIGs with respect to the systemic velocities of the parent galaxies from which they emanate increase almost monotonically with the distance from the nucleus of the respective galaxies, reaching ~ -400 to -800 km s^{-1} at around 40–80 kpc from the galaxies. The one-sided morphologies and the velocity fields of the EIGs are consistent with the predictions of numerical simulations of ram pressure stripping. We found a very low velocity filament ($v_{\rm rel} \sim -1300$ km s^{-1}) at the southeastern edge of the disk of IC 4040. Some bright compact knots in the EIGs of RB 199 and IC 4040 exhibit blue continuum and strong Hα emission. The equivalent widths of the Hα emission exceed 200 Å and are greater than 1000 Å for some knots. The emission-line intensity ratios of the knots are basically consistent with those of sub-solar abundance H II regions. These facts indicate that intensive star formation occurs in the knots. Some filaments, including the low-velocity filament of the IC 4040 EIG, exhibit shock-like emission-line spectra, suggesting that shock heating plays an important role in ionization and excitation of the EIGs.

Key words: galaxies: clusters: individual (Coma) – galaxies: clusters: intracluster medium – galaxies: evolution – galaxies: kinematics and dynamics – intergalactic medium

Online-only material: color figures

1. INTRODUCTION

Clusters of galaxies are ideal laboratories for investigating environmental effects in galaxy evolution. The extreme environments of the clusters—the high number density of galaxies, strong gravitational field, and dense hot gas filling intergalactic space—allow us to study how these environmental factors affect the evolution of cluster member galaxies. A substantial body of observational evidence suggests that cluster environment significantly affects cluster galaxy evolution, for example, the morphology–density relation (Dressler 1980, 1994; Postman & Geller 1984; van der Wel et al. 2007), the redshift–blue-galaxy fraction relation (Butcher & Oemler 1978, 1984), or the density–H I-deficiency relation (Cayatte et al. 1990, 1994; Solanes et al. 2001). Researchers have proposed various physical mechanisms potentially responsible for these observational facts (Boselli & Gavazzi 2006), including galaxy–galaxy interaction (Byrd & Valtonen 1990), galaxy harassment (Moore et al. 1996), tidal interaction between galaxies and cluster potential (Byrd & Valtonen 1990; Henriksen & Byrd 1996), galaxy starvation (Bekki & Couch 2003), and ram pressure stripping (Gunn & Gott 1972; hereafter referred as to RPS).

Although it is not clear which mechanism plays the most important role in the morphological and color evolution of cluster galaxies, it is at least certain that rapid removal of the interstellar gas of galaxies is a key factor (Okamoto & Nagashima 2003; van Gorkom 2004; Boselli et al. 2008; van der Wel et al. 2010). In particular, RPS caused by fast interaction between galaxies and the hot intracluster medium (ICM) must play a very important role in gas removal (Vollmer et al. 2001b; Fujita 2004; Vollmer 2009; Cortese et al. 2011) and in star formation enhancement in the galaxies (Fujita & Nagashima 1999; Schulz & Struck 2001). A number of observational studies have focused on this subject. The H I gas of galaxies is systematically deficient in the cores of nearby rich clusters (Cayatte et al. 1990, 1994; Bravo-Alfaro et al. 2000, 2001). Deep H I imaging revealed one-sided H I gas flows around late-type galaxies in the Virgo Cluster (Oosterloo & van Gorkom 2005; Chung et al. 2007, 2009). Asymmetric distributions of molecular gas found in some cluster galaxies also suggest that the molecular gas is affected by ram pressure from the hot ICM (Vollmer et al. 2001a, 2008, 2009; Vollmer & Huchtmeier 2003; Sivanandam et al. 2010). Recently, elongated X-ray gas flows from galaxies have been found in nearby clusters (Sun et al. 2007, 2010; Randall et al. 2008). In addition, many case studies have focused on ionized gas flows from cluster member galaxies probed by Hα emission (Kenney & Koopmann 1999; Gavazzi et al. 2001, 2003; Yoshida et al. 2002, 2004; Sakai et al. 2002; Koopmann & Kenney 2004; Chemin et al. 2005; Cortese et al. 2006; Kenney et al. 2008). Some pieces of evidence of dust stripping in the Virgo galaxies have also been reported (Crowl et al. 2005; Abramson et al. 2011).

We serendipitously discovered a number of very extended ionized gas (EIG) filaments around the member galaxies of the Coma Cluster (Yagi et al. 2007; Yoshida et al. 2008, hereafter YY08; Yagi et al. 2010, hereafter YY10). The filaments are

* Based on data collected at the Subaru Telescope, which is operated by the National Astronomical Observatory of Japan.

extended toward one side of the parent galaxies (YY10). The most remarkable example of the one-sided extension is the 60 kpc straight Hα filament found around D100 (Yagi et al. 2007). Another interesting object is the complex of ionized gas filaments, star-forming blue knots, and young stellar filaments extended from an E+A galaxy RB 199 ("fireballs"; YY08). The morphology of the latter very much resembles strings of compact blue knots around the two galaxies falling into $z \approx 0.2$ clusters found by Cortese et al. (2007). Cortese et al. (2007) interpreted these peculiar features as star-forming regions in the gas stripped from the parent galaxies by the combined action of tidal interaction and RPS. The fireballs are a low-redshift counterpart of these features (YY08). Recently, Hester et al. (2010) reported a similar structure around a low surface brightness galaxy IC 3418 in the Virgo Cluster (see also Fumagalli et al. 2011).

YY10 found some properties specific to the EIGs' parent galaxies. The radial velocities of the parent galaxies are distributed either at the blue or at the red edge of the velocity distribution of Coma member galaxies. In addition, almost all the parent galaxies have blue colors; about 60% of the parent galaxies are distributed well below (bluer side) from the color–magnitude relation (red sequence) of the early-type galaxies of the Coma Cluster. These facts suggest that the parent galaxies are late-type galaxies that have recently fallen into the cluster. They have not yet been well processed in the cluster environment. Further, YY10 classified the EIGs into three categories: (1) disk star formation + connected Hα gas, (2) no disk star formation with connected Hα gas, and (3) detached Hα gas.

Smith et al. (2010) found on *Galaxy Evolution Explorer* (*GALEX*) images one-sided UV tails around a number of Coma member galaxies whose morphologies resemble the EIGs. More than half of their objects overlapped the EIG galaxies discovered by YY10. They assessed the statistical characteristics of these UV tail galaxies and concluded that these galaxies are newcomers to the Coma Cluster (Smith et al. 2010). Good correlation between the EIGs and the UV tails suggests that these two kinds of features were created by the same mechanism; the most plausible one is RPS. Furthermore, this indicates that active star formation occurs in the stripped gas in the cluster environment.

Here we present the results of optical spectroscopic observations of the EIGs around four Coma member galaxies. We assumed that the cosmological parameters $(h_0, \Omega_m, \Omega_\lambda) = (0.73, 0.24, 0.72)$ and the distance modulus of the Coma Cluster is 35.05 (Yagi et al. 2007). The linear scale at the Coma Cluster is 474 pc arcsec^{-1} under this assumption.

2. OBSERVATION AND DATA REDUCTION

Deep spectroscopic observations of four Coma member galaxies, RB 199, IC 4040 (GMP 2559), GMP 2923, and GMP 3071, were performed using the faint object spectrograph FOCAS (Kashikawa et al. 2002) attached to the Subaru Telescope on 2009 May 20. Two multi-slit masks for each of RB 199 and IC 4040 were used to cover the complicated structure of the emission-line regions over as wide an area as possible. GMP 2923 and GMP 3071 were observed using one multi-slit mask. The positions and lengths of the slits are shown in Figures 1–4. The width of each small slit was 0.″8. The lengths of the slits ranged from 10″ to 30″. A 300 groove mm^{-1} grism, whose straight light travel wavelength is 6500 Å, was used. The FWHM of the sky emission lines around 6700 Å is 7.8 Å, which means that the spectral resolving power R of our spectroscopy

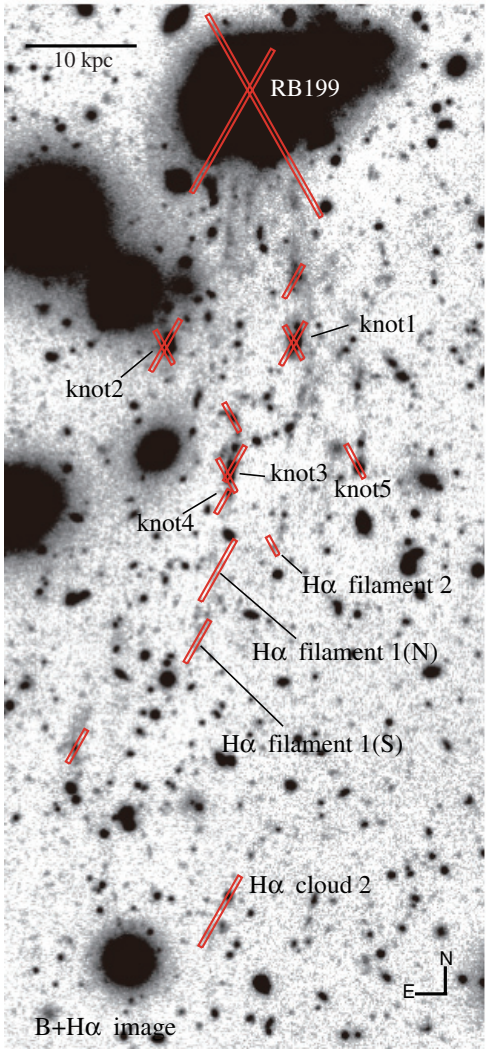

Figure 1. Slit positions of the spectroscopy of the extended ionized gas (EIG) of RB 199 ("fireballs"; YY08) overlaid on a composite image of the Hα narrowband and B-band images. All the images used in Figures 1–4 were taken with Suprime Cam attached to Subaru Telescope. Details of the observations of these images were described previously in YY10.

(A color version of this figure is available in the online journal.)

is 850 (the velocity resolution is about 350 km s^{-1}) over the Hα region. Table 1 presents the observation log.

Data reduction was performed in the standard manner. The bias level of each frame was estimated with the average count of the over-scan region of the CCD and then subtracted from each frame. Flat-fielding was done using dome flat frames. Wavelength calibration was performed using sky emission lines. The rms residual of wavelength fitting for sky lines was 0.14 Å in the wavelength region of 6000–7000 Å. Because there are no strong sky emission lines blueward of 5500 Å, wavelength calibration is not accurate as in the longer wavelength region. The rms error was 0.3 Å at 5300 Å. Thus, we measured the radial velocities of the EIGs using the Hα line only.

Flux calibration was initially conducted using spectrophotometric standard star data. However, the standard star data were taken with an order sorting filter (Y47) whose cutoff wavelength was 4700 Å, while the filter was not used for the observation of the EIGs. Thus, we had to correct the transmission curve of Y47 to ensure accurate flux calibration for the wavelength region blueward of 4700 Å. We divided the initial

Table 1
Spectroscopy Observation Log

Mask ID	Object	Center	P.A.	Exposure
MS0631	IC 4040	$13^h00^m43^s.2$ +28°03′06″	215°	6 × 600 s
MS0632	IC 4040	$13^h00^m38^s.4$ +28°04′42″	125°	3 × 300 s + 3 × 600 s
MS0632-off	IC 4040	$13^h00^m38^s.6$ +28°04′45″	125°	1 × 600 s
MS0634	RB 199	$12^h58^m43^s.3$ +27°46′19″	150°	6 × 600 s
MS0635	RB 199	$12^h58^m38^s.7$ +27°44′35″	210°	6 × 600 s
MS0636	GMP 2923, 3071	$12^h59^m58^s.4$ +27°44′58″	60°	2 × 600 s

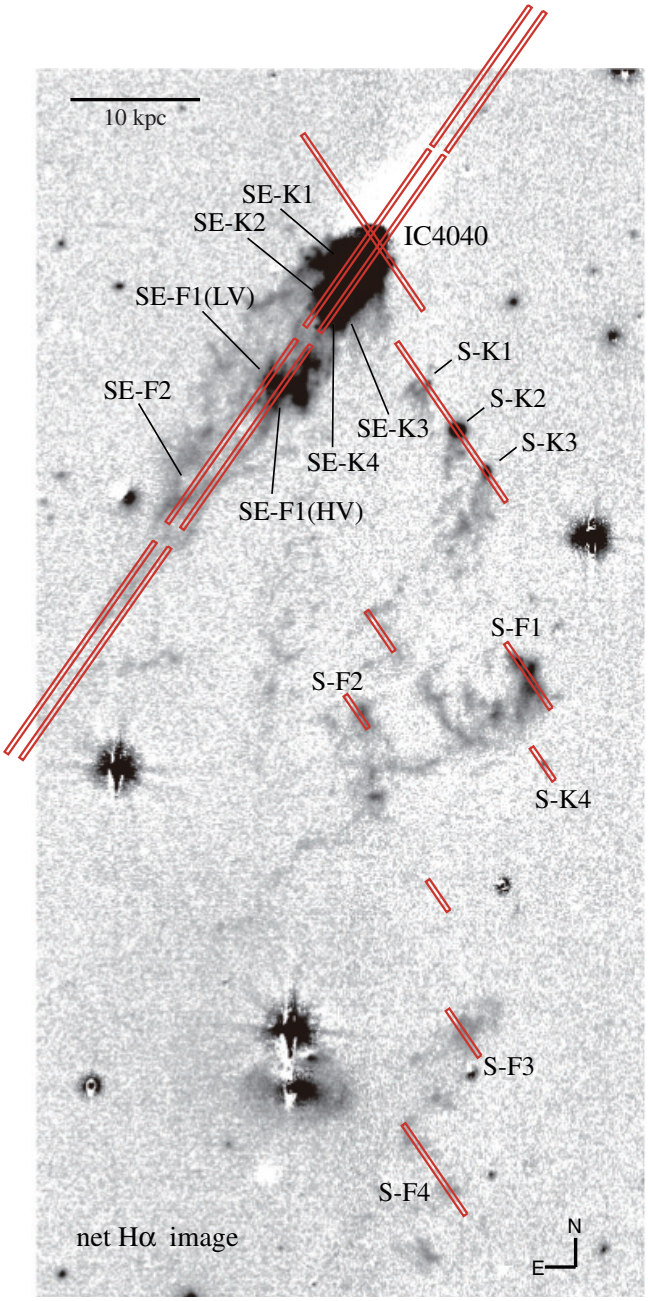

Figure 2. Slit positions of the spectroscopy of the EIG of IC 4040 overlaid on the net Hα image.
(A color version of this figure is available in the online journal.)

flux-calibrated frames by the transmission curve of Y47, which was normalized to 1 at the maximum transmission wavelength (6000 Å). We checked validity of the above recalibration procedure by comparing the calibrated spectrum of an elliptical galaxy (SDSS J125845.26+274655.0) taken with one slit of the mask MS0635 with the spectra of eight early-type galaxies listed in Kennicutt (1998). The type of the reference galaxies ranges from E0 to S0. All the spectra were normalized at 6000 Å. The rms relative difference between the spectrum of our E galaxy and the spectrum of each reference early-type galaxy was less than 7% for the wavelength region between 4300 Å and 7000 Å. Thus, we adopted that the recalibration we made was correct enough for further analysis. The signal-to-noise ratio of the measured spectra shorter than 4300 Å was too low to enable confident comparison, so we do not include spectra shorter than 4300 Å in the following analysis and discussion.

We fitted Gaussian functions to the emission lines to measure the fluxes and the velocities of the lines. Although it was difficult to measure velocity dispersion accurately because of the low spectral resolution of our spectra, we obtained rough estimation of the velocity dispersion σ by applying a simple decomposition scheme; $\sigma = \sqrt{\sigma_{\rm obs}^2 - \sigma_{\rm sky}^2}$, where $\sigma_{\rm obs}$ and $\sigma_{\rm sky}$ are the dispersions of the Gaussian functions fitted to the observed emission line and that of the sky line, respectively ($f(\lambda) \propto \exp(-\lambda^2/2\sigma^2)$; $\sigma = {\rm FWHM}/2\sqrt{2\ln 2}$). One spectral resolution unit was sampled with eight pixels of the CCD. This oversampling enabled us to measure the emission-line widths with an accuracy at 10% of the FWHM of the sky lines. Since the FWHM of the sky lines was 7.8 Å, we resolved the emission lines whose FWHMs were wider than 8.6 Å, which means that the lower limit of σ we could measure was ≈70 km s^{-1} at 6700 Å.

Imaging data of the target galaxies in deep narrowband Hα and broadband B and $R_{\rm C}$ bands used in this paper are those presented in YY10 for morphological study of the EIGs around these galaxies. They were taken using Suprime Cam (Miyazaki et al. 2002) attached to the Subaru Telescope. The data were collected over three observing runs from 2006 to 2009. See YY10 for the details of the imaging observations and data reduction.

3. RESULTS

3.1. The Morphologies and Kinematics of the EIGs

The overall morphological characteristics of the EIGs of our target galaxies were previously reported by YY10. Here, we describe in detail the morphologies of the EIGs and present their velocity fields newly revealed by our spectroscopy for each target galaxy.

3.1.1. RB 199

The B, $R_{\rm C}$, and Hα images of RB 199 were shown in our previous work (YY08). The characteristics of the EIG (fireball) of RB 199 can be summarized as follows: (1) the EIG consists of a number of bright star-forming knots, elongated blue filaments, and more extended Hα emitting gas. Total length of the EIG is

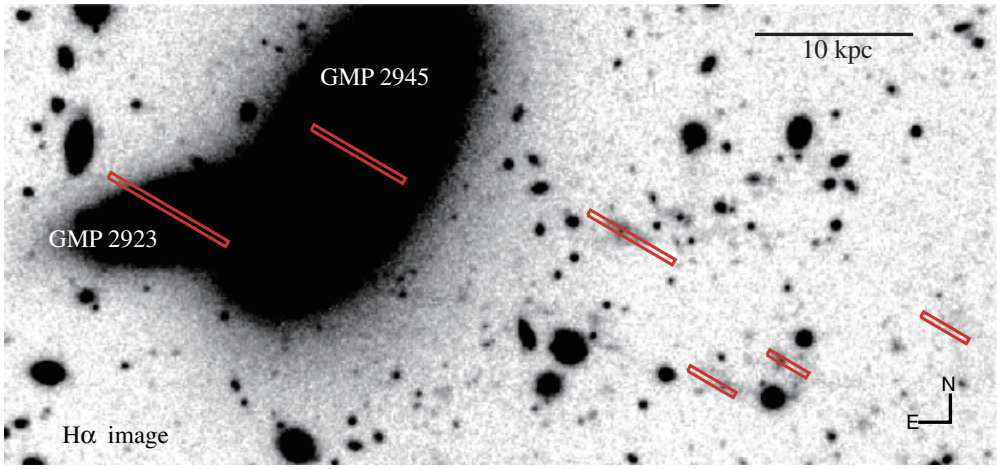

Figure 3. Slit positions of the spectroscopy of the EIG of GMP 2923 overlaid on the Hα narrowband image.
(A color version of this figure is available in the online journal.)

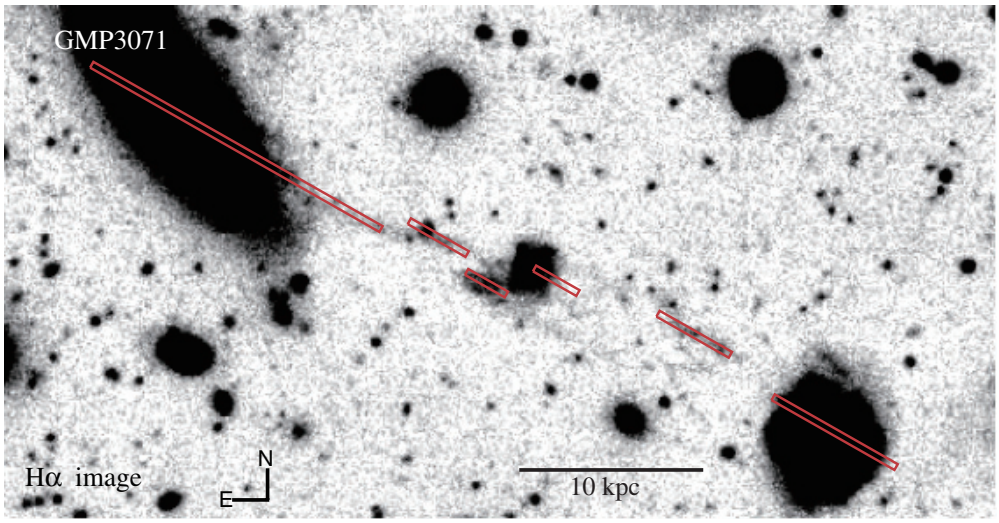

Figure 4. Slit positions of the spectroscopy of the EIG of GMP 3071 overlaid on the Hα narrowband image.
(A color version of this figure is available in the online journal.)

about 80 kpc. (2) The absolute magnitudes of the bright knots range from −12 to −13 mag, which are comparable to nearby dwarf galaxies. (3) The bright knots emit both blue continuum light and Hα emission. The Hα emitting regions are offset from the peak of the blue continuum emission. (4) The blue filaments are connected to the main body of the galaxy, while the Hα filaments are connected to the tips of the blue filaments. (5) The bright knots and blue filaments are detected in UV light by the *GALEX* satellite.

Figure 5 shows the velocity field of the EIG of RB 199. Relative radial velocities of the EIG filaments with respect to the systemic velocity of RB 199 increase with the distance from the nucleus at almost a constant rate of -7 km s^{-1} kpc^{-1}. The relative radial velocity of the most distant cloud of the EIG, Hα cloud 2 (YY08), is roughly consistent with the extrapolation of the line of constant increase, which suggests that this cloud is really a part of the EIG.

We found that a faint Hα component with a velocity of ≈6250 km s^{-1} overlaps along the line of sight to Hα cloud 2. Figure 6 shows the velocity field of the RB 199 EIG with this slow-velocity (SV) component. The velocity of this SV component is slightly lower than that of the mean velocity (≈6900 km s^{-1}) of the Coma Cluster. The velocity difference between the SV component and Hα cloud 2 is ∼2000 km s^{-1}, suggesting that the SV component is not associated with the RB 199 EIG.

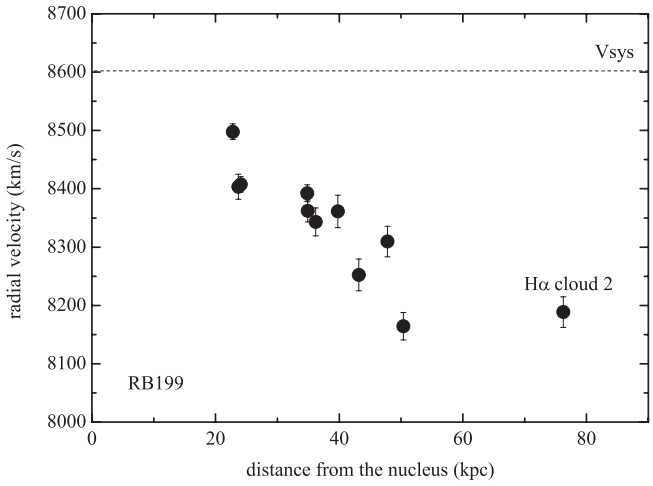

Figure 5. Velocity field of the EIG of RB 199. The systemic velocity of the galaxy is determined by the Hα absorption line of the nucleus.

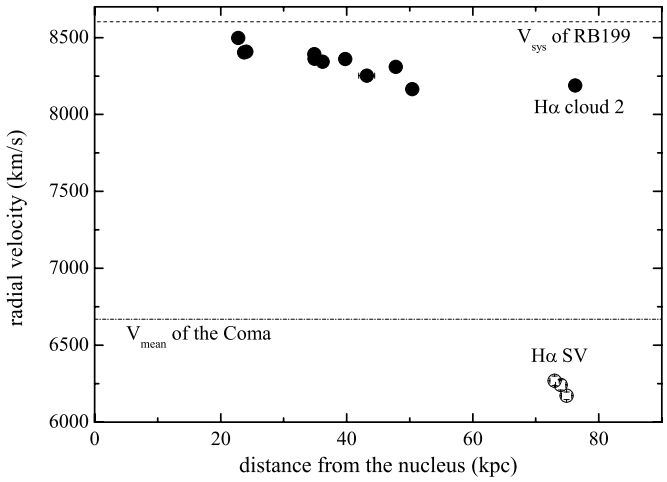

Figure 6. Velocity fields of the EIG of RB 199 and the low-velocity filaments overlapping Hα filament 2.

3.1.2. IC 4040

Figure 7 presents a pseudo-color image (blue, green, and red colors represent B, R_C, and Hα images, respectively) of the spiral galaxy IC 4040 taken with Subaru Suprime Cam (YY10, reproduced by permission of the American Astronomical Society, AAS). The figure clearly shows a very EIG expelled from the galaxy disk.

The structure of the EIG is very complicated. Two major streams extend toward the southeast and south from the galaxy. The southeast stream of the EIG is elongated almost linearly along the major axis of the galaxy, and its root is connected to the nuclear star-forming region. This southeast stream reaches ∼50 kpc from the nucleus. Figure 8 shows the detailed structure of the central bright part of the EIG. The nucleus of the galaxy is surrounded by several bright star-forming knots. This complex of the star-forming regions is truncated at the northwestern side of the nucleus. The shape of the ionized gas distribution indicates a large-scale bow shock and a giant gas flow toward the southeast from the nucleus. The opening angle of the gas

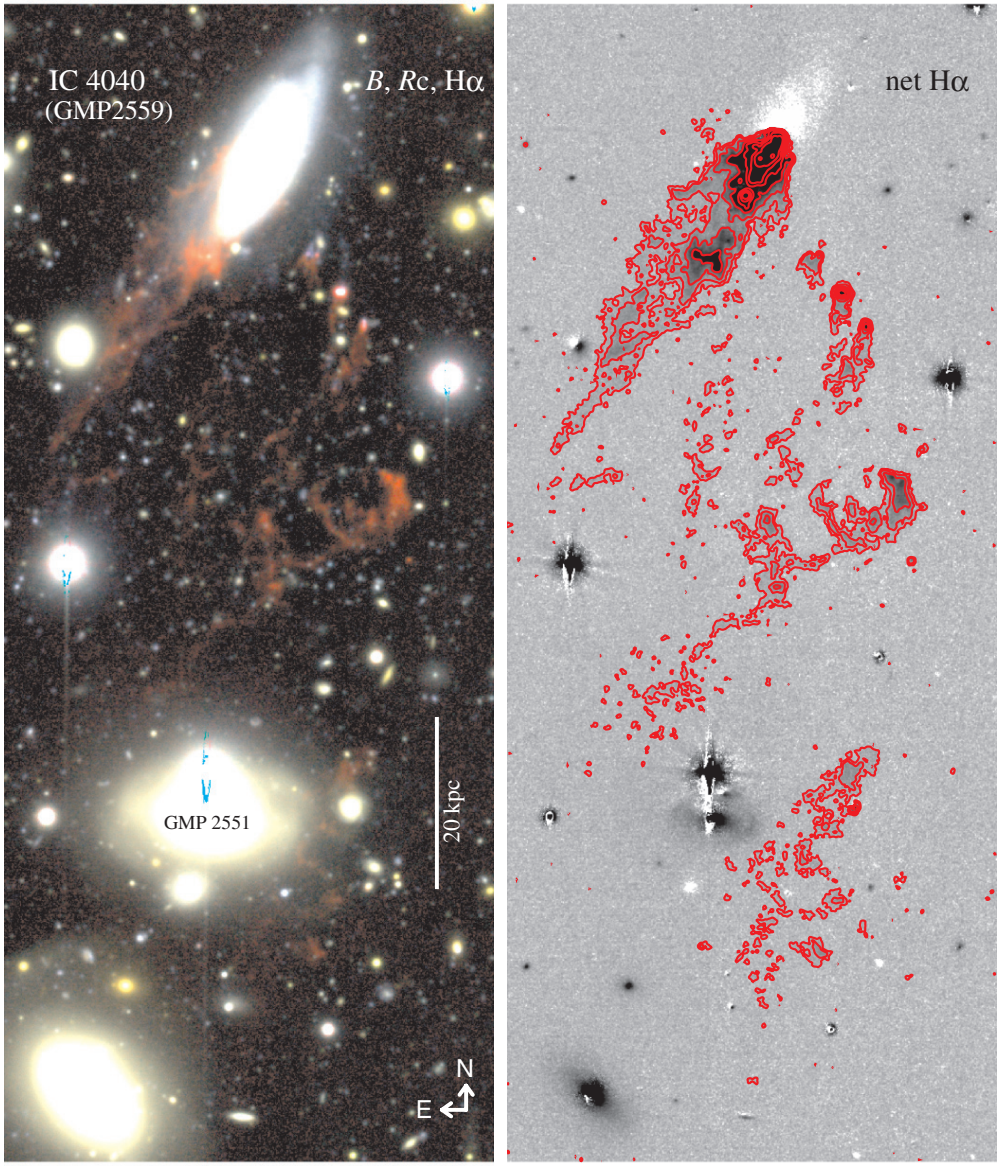

Figure 7. Pseudo-color image (B, R_C, and Hα composite: left panel) and net Hα image (right panel) of IC 4040. This figure is reproduced from YY10 by permission of the AAS.

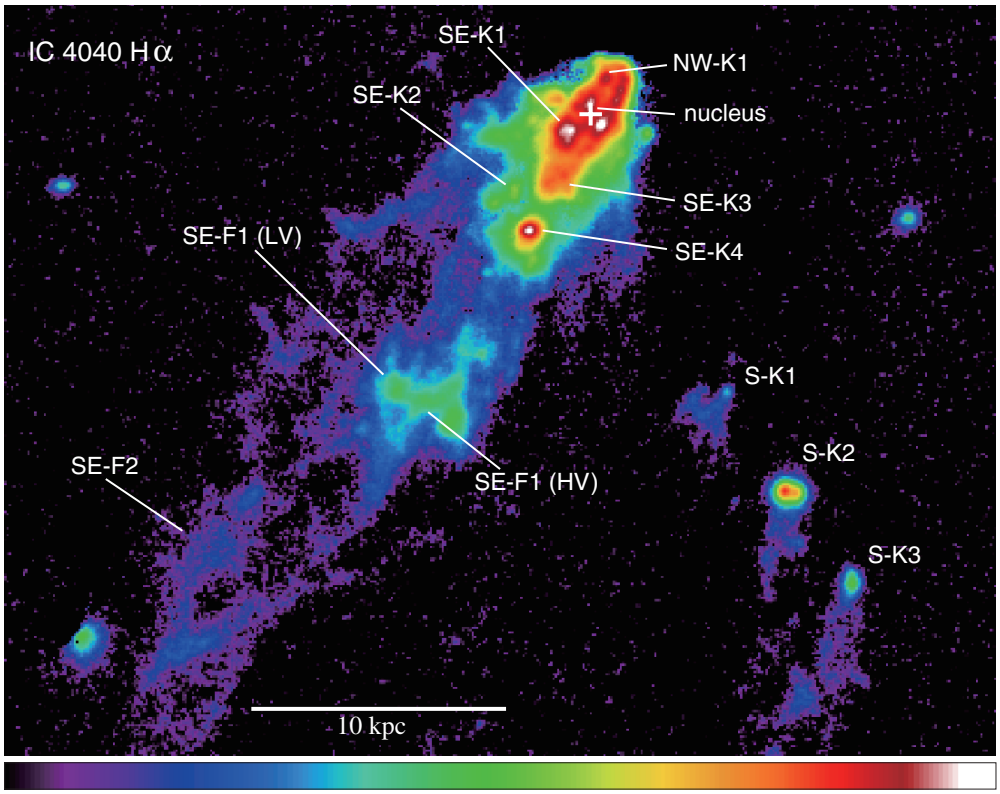

Figure 8. Details of the morphology of the Hα emitting gas of IC 4040 around the galaxy disk and nucleus. In the central region of the galaxy, several bright Hα knots and complicated structure of ionized gas filaments/clouds can be seen. The Hα gas is truncated at the northwestern side and exhibits bow-shock-like morphology.

flow is about 65° and almost symmetric with respect to the major axis of the galaxy. Several bright Hα knots (NW-K1, SE-K1, etc.; see Figure 8) surround the nucleus. The brightest one, SE-K4, has a size of $r \sim 0.5$ kpc and is located at 7 kpc from the nucleus. A large complex of diffuse Hα clouds/filaments appears at around 15 kpc from the nucleus. Farther away, a tangle of several filaments, with typical width of 1 kpc, extends out to 50 kpc. For convenience, we refer to the large complex and the filaments between 20 kpc and 30 kpc as SE-F1 and SE-F2, respectively. As described later, our spectroscopic observations revealed that the SE-F1 consists of at least two kinematically different components, a low-velocity (LV) component and a high-velocity (HV) component.

The $B - R_C$ color image shown in Figure 9 reveals that the southeast stream is very dusty. The close spatial correlation between the dust and the EIG and the one-sided morphology of the dust suggest that the ionized gas and the dust are stripped together and are mixed with each other in the stripped flow. Both the dust stream and the southeast part of the EIG extend in the same direction as the H I gas tail found by Bravo-Alfaro et al. (2000, 2001). A recent far-infrared/submillimeter survey of the Virgo Cluster with *Herschel* revealed that dust disks are truncated in H I deficient galaxies (Cortese et al. 2010). These results suggest that dust in galaxies can be stripped in the cluster environment. The dust stream in IC 4040 exemplifies a dust stripping site observed in a cluster.

The EIG is widely distributed south of IC 4040. The southern part of the EIG consists of three conspicuous bright knots (S-K1, S-K2, and S-K3; see Figure 2), several giant complexes of clouds/filaments (S-F1, S-F2, etc.), and many small filaments.

The three bright knots are blue in color. These features have been detected in the UV light with *GALEX* (Smith et al. 2010). Of the three knots, knot 2 is the brightest. Smith et al. (2010) observed a Wolf–Rayet feature in their Keck spectrum, suggesting that this knot is very young (younger than 5 Myr). Elongated Hα filaments are connected to these knots. All the connected filaments have head-tail morphologies whose position angles are the same as the southeast stream.

Many ionized gas clouds/filaments are distributed over 30 kpc × 80 kpc in the southern area of IC 4040. The brightest one is a thick loop-like filament at about 40 kpc from the galaxy (S-F1 in Figure 2). S-F2 is another bright filament connected to S-F1. S-F3 and S-F4 are diffuse filaments seen near an early-type galaxy GMP 2551 (Figure 7). Other than these filaments, many small filaments are seen between S-F2 and IC 4040.

Figure 10 shows the velocity field of the EIG of IC 4040. The brightness of the EIG of IC 4040 allowed us to trace the velocity field along each slit. The IC 4040 EIG has a velocity field similar to that of the RB 199 EIG; the relative radial velocities of the filaments increase almost monotonically with the distance from the nucleus (Figure 10). Within 5 kpc of the nucleus, the Hα gas along the galaxy major axis follows the galaxy rotation. The acceleration of the EIG begins at 5 kpc from the nucleus. The overall acceleration rate in a range of 5–80 kpc is ~ -10 km s^{-1} kpc^{-1}.

We noted several peculiar features in the velocity field of the IC 4040 EIG. The most remarkable one is a very low velocity component at ∼12 kpc from the nucleus. This component is spatially associated with the SE-F1 (see Figure 2); we call it SE-F1 (LV). The relative velocity of the SE-F1 (LV) is -1300 km s^{-1} with respect to the systemic velocity of the galaxy. Its velocity dispersion reaches ≈800 km s^{-1} (Figure 11). In contrast, the southwest side of the SE-F1 is much faster than the SE-F1 (LV) and almost follows the overall motion of the EIG. This fast component, called SE-F1 (HV), has a

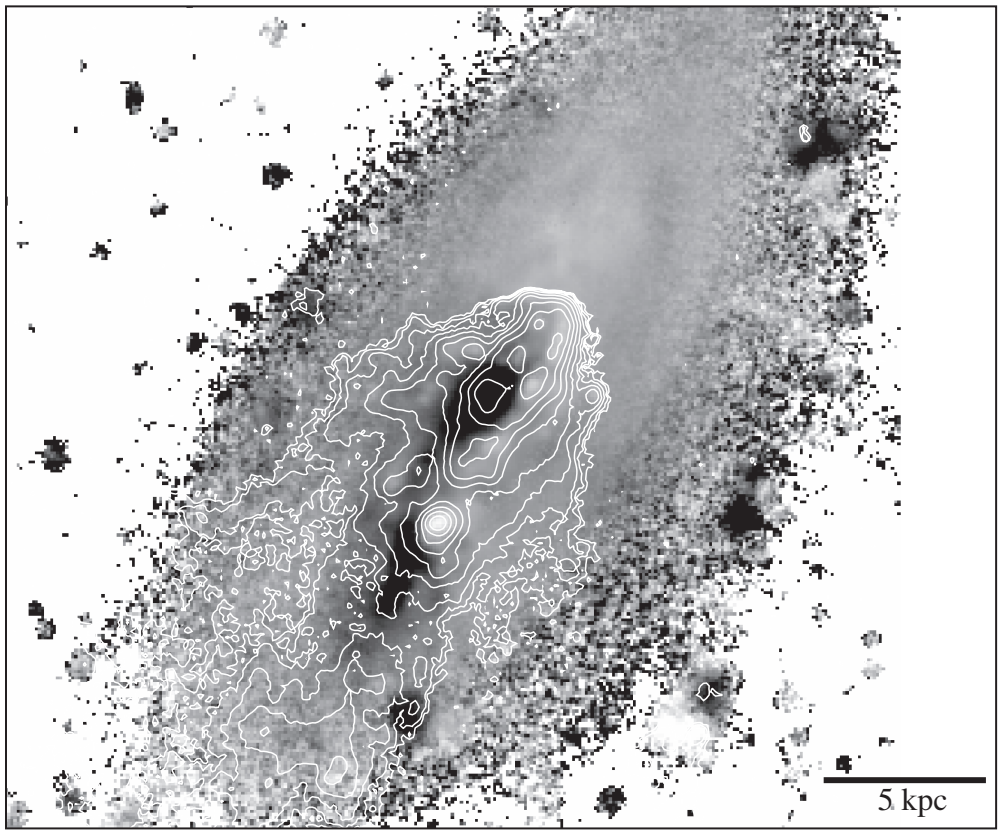

Figure 9. $B - R_C$ color image (gray scale) of IC 4040. The darker color represents a larger $B - R_C$. A contour map of the Hα gas distribution is overlaid on the $B - R_C$ image.

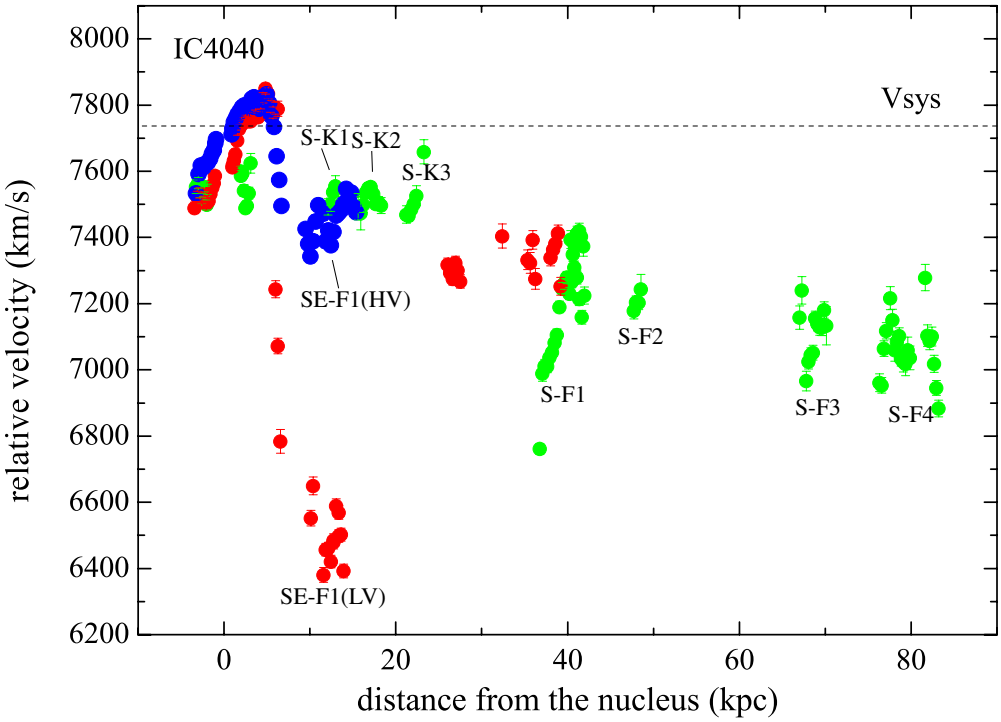

Figure 10. Velocity field of the EIG of IC 4040. Green dots, blue dots, and red dots represent the data points of the slit masks of MS0631, MS0632, and MS0632-off, respectively.

(A color version of this figure is available in the online journal.)

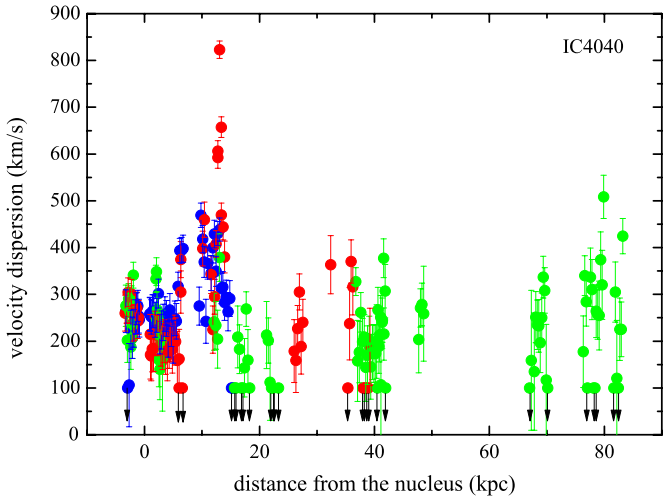

Figure 11. Velocity dispersion of the EIG of IC 4040. The color difference is the same as in Figure 10.

(A color version of this figure is available in the online journal.)

relative velocity of ≈−300 km s^{-1} and a velocity dispersion of ≈400 km s^{-1}. Figure 12 shows the two-dimensional spectra of the circumnuclear Hα gas and the southeast filaments. In this figure, large velocity shift and wide velocity dispersion of SE-F1 (LV) are clearly seen.

The S-F1 has a large velocity gradient (∼70 km s^{-1} kpc^{-1}) within it. The filament has a relative velocity of ≈−700 km s^{-1} at the edge of the galaxy. At the opposite edge, the relative velocity reaches −450 km s^{-1}. The S-F3 and S-F4 are highly turbulent, and the velocity dispersions are ∼200–400 km s^{-1}.

3.1.3. GMP 2923 and GMP 3071

The EIG around GMP 2923 is shown in Figure 4(d) in YY10. Two galaxies—GMP 2923 and GMP 2945—overlap in the line of sight near the EIG (Figure 3). We measured the radial velocity of the early-type galaxy GMP 2945 with the same slit mask as that used for the EIG; it is 6500 km s^{-1}, much slower than those of the EIG and GMP 2923. Thus, GMP 2945 is kinematically independent from the EIG.

The EIG of GMP 2923 is characterized by two knotty straight streams (see Figure 4(d) in YY10). The opening angle of the

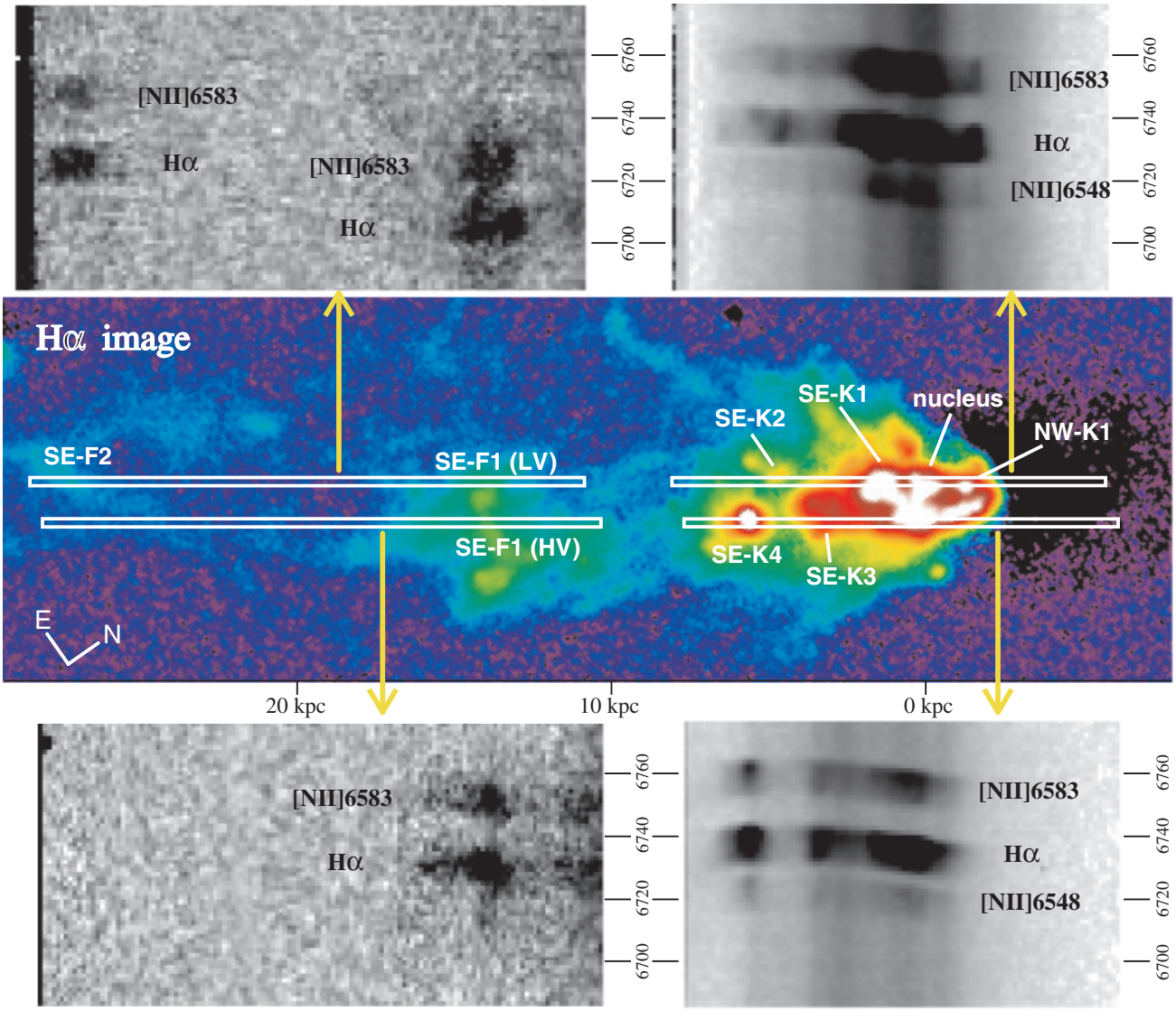

Figure 12. Two-dimensional spectra of the SE filaments and the nuclear H II regions of IC 4040. The middle panel shows a pseudo-color image of the Hα emitting filaments.

(A color version of this figure is available in the online journal.)

Table 2
Emission-line Fluxes and Intensity Ratios of the EIGs

ID	Distance[a]	Length[b]	$f_{H\alpha}$[c]	$f_{H\beta}$[d]	[N II]/Hα[e]	[S II]/Hα[e]	[O I]/Hα[e]	[O III]/Hβ[e]
IC 4040								
Nucleus	...	0.59	271	85.3	-0.47 ± 0.01	-0.52 ± 0.01	-1.60 ± 0.01	-0.36 ± 0.01
NW-K1	1.2	0.44	221	51.2	-0.48 ± 0.01	-0.61 ± 0.01	-1.69 ± 0.02	-0.54 ± 0.01
SE-K1	1.1	0.74	303	53.6	-0.32 ± 0.01	-0.57 ± 0.01	-1.36 ± 0.01	-0.43 ± 0.01
SE-K2	3.8	0.90	47.1	17.1	-0.40 ± 0.01	-0.44 ± 0.01	-1.22 ± 0.03	-0.51 ± 0.03
SE-K3	2.5	0.74	107	23.9	-0.43 ± 0.01	-0.58 ± 0.01	-1.42 ± 0.02	-0.27 ± 0.01
SE-K4	4.8	0.74	194	37.1	-0.51 ± 0.01	-0.61 ± 0.01	-1.61 ± 0.02	-0.17 ± 0.01
S-K1	12.3	0.59	2.1	...	-0.49 ± 0.10	-0.12 ± 0.07	-0.48 ± 0.10	...
S-K2	17.0	0.74	172	59.1	-1.04 ± 0.01	-1.05 ± 0.01	-1.98 ± 0.04	0.50 ± 0.01
S-K3	21.7	0.74	14.6	5.3	-0.37 ± 0.02	-0.40 ± 0.02	-1.41 ± 0.12	-0.05 ± 0.04
S-K4	47.9	0.74	3.2	...	...	...	...	...
SE-F1(LV)	12.8	2.22	16.4	3.9	-0.12 ± 0.03	-0.51 ± 0.09	-0.64 ± 0.09	0.04 ± 0.13
SE-F1(HV)	13.8	3.11	28.4	3.4	-0.16 ± 0.03	-0.38 ± 0.06	-0.63 ± 0.06	0.12 ± 0.21
SE-F2	26.7	1.78	14.8	...	...	...	...	...
S-F1N	37.8	0.59	5.7	2.1	-0.44 ± 0.04	-0.27 ± 0.04	-0.77 ± 0.07	-0.42 ± 0.15
S-F1S	39.2	0.74	5.5	2.1	-0.47 ± 0.05	-0.42 ± 0.06	-0.90 ± 0.11	-0.36 ± 0.18
S-F2	40.9	1.04	2.8	...	-0.25 ± 0.08	-0.27 ± 0.10	...	...
S-F3	68.8	2.37	6.3	...	-1.08 ± 0.22	...	...	...
RB 199								
Knot 1	22.8	1.18	23.5	8	-1.02 ± 0.03	-0.67 ± 0.02	-1.52 ± 0.11	0.19 ± 0.02
Knot 1e	23.7	1.04	3.8	0.7	-1.06 ± 0.33	-0.24 ± 0.09	-0.61 ± 0.14	-0.25 ± 0.44
Knot 2	24.1	1.48	37.9	13	-0.86 ± 0.02	-0.29 ± 0.01	-1.06 ± 0.03	0.07 ± 0.02
Knot 3	34.8	0.89	4.9	2	-0.92 ± 0.09	-0.26 ± 0.03	-0.99 ± 0.10	-0.22 ± 0.11
Knot 4	36.2	0.74	1.9	...	...	...	...	...
Knot 5	34.9	1.04	21.6	8	-1.14 ± 0.06	-0.65 ± 0.03	-1.45 ± 0.12	0.37 ± 0.02
Hα filament 1(N)	43.2	2.51	1.3	...	...	...	...	...
Hα filament 1(S)	50.4	1.18	2.4	...	...	...	...	...
Hα filament 2	39.8	0.89	2.7	...	...	...	...	...
Hα cloud 2	76.3	1.48	1.9	...	...	...	...	...

Notes.
[a] Distance from the nucleus of the parent galaxy in units of kpc.
[b] Length along the slit in units of kpc.
[c] Hα flux in units of 10^{-17} erg s^{-1} cm^{-2}.
[d] Hβ flux in units of 10^{-17} erg s^{-1} cm^{-2}.
[e] Logarithmic value of the emission-line intensity ratio.

streams is $\approx 20^{\circ}$. The root of the streams is detached from the galaxy. The EIG is extended to $\sim$50 kpc from GMP 2923.

The EIG of GMP 3071 consists of slightly wiggled narrow filaments (Figure 4(f) in YY10). The root of the EIG is connected to the nucleus of the galaxy. The angle between the galaxy major axis and the EIG is $\approx 40^{\circ}$, and the length of the EIG is $\sim$25 kpc.

The kinematics of both the GMP 2923 and GMP 3071 EIGs also reveal a monotonically increasing pattern. Figures 13 and 14 show the velocity fields of the EIGs of the two galaxies. The acceleration rates are ≈ -10 km s^{-1} kpc^{-1} and ≈ -25 km s^{-1} kpc^{-1} for GMP 2923 and GMP 3071, respectively.

The kinematics of the EIG of GMP 3071 is rather complex in the galaxy disk, showing a rapid drop and rise whose amplitude is $\approx$200 km s^{-1} (Figure 14). The net Hα image taken by YY10 revealed that the ionized gas near the nucleus has a wiggled chain of small blobs. Together with the kinematics, this may suggest a helical motion of the ionized gas caused by the stripping force coupled with galactic rotation.

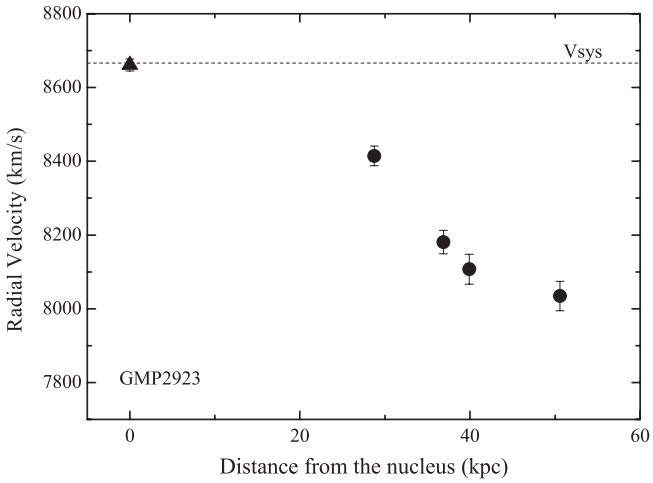

Figure 13. Velocity field of the EIG of GMP 2923.

3.2. Excitation of the EIGs

Most of the EIG extended filaments are too faint to detect emission lines other than Hα. We could detect diagnostic emission lines such as [S II] or [N II] only in bright knots and some bright filaments in the EIGs of RB 199 and IC 4040. Table 2 summarizes the measured fluxes of the emission lines for bright parts of the EIGs of RB 199 and IC 4040.

Figure 15 shows the spectra of the bright knots and the nucleus of RB 199. The bright knots of RB 199 are characterized

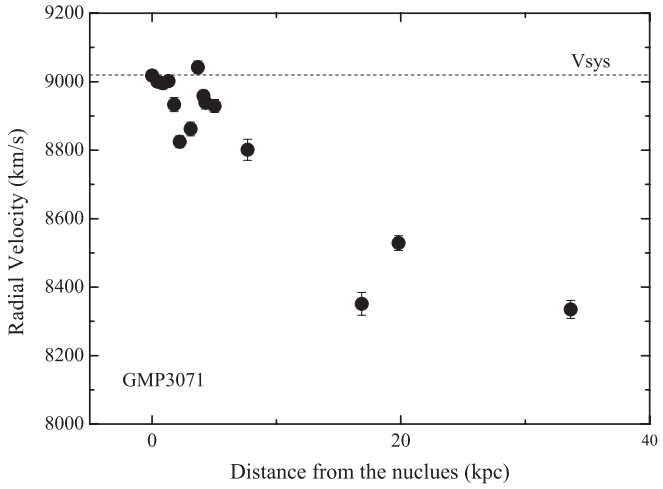

Figure 14. Velocity field of the EIG of GMP 3071.

by strong emission lines and blue continuum. The equivalent widths of Hα are 310 Å, 230 Å, and 1500 Å for knots 1, 2, and 5, respectively. The most interesting feature of the bright knot spectra is the weak [N II] λ6548/λ6583 emission. In knot 2 or knot 3, [S II] λ6717/λ6731 lines are stronger than [N II]. In knot 3, even [O I] λ6300 is stronger than [N II]. In knot 1 and knot 5, very weak [N II], [S II], and [O I] and relatively strong [O III] λ5007 indicate that these knots are metal-deficient H II regions. The spectra of knot 2 and knot 3 reveal strong [S II] and [O I] lines, suggesting that shock heating contributes the gas excitation. The nucleus of RB 199 has a spectrum typical of post-starburst galaxies (Poggianti et al. 2004). It is characterized by strong Balmer absorption lines, very weak metal-absorption lines, and a blue continuum.

Figure 16 shows the spectra of the bright knots and filaments of the EIG of IC 4040 with the nuclear spectrum of IC 4040 itself. The spectrum of S-K2 of the IC 4040 EIG is that of a typical metal-poor star-forming region. The Hα line is very strong in S-K2; the equivalent width reaches $\sim$1000 Å. In the blue region of the spectrum, we confirmed a weak Wolf–Rayet feature (Figure 17), which was found by Smith et al. (2010). S-K3 shows relatively strong [N II] and [S II], suggesting that shock excitation may play a role in the gas excitation. The spectra of the nucleus and S-K4 resemble each other, while the continuum of S-K4 is redder than that of the nucleus. It reflects

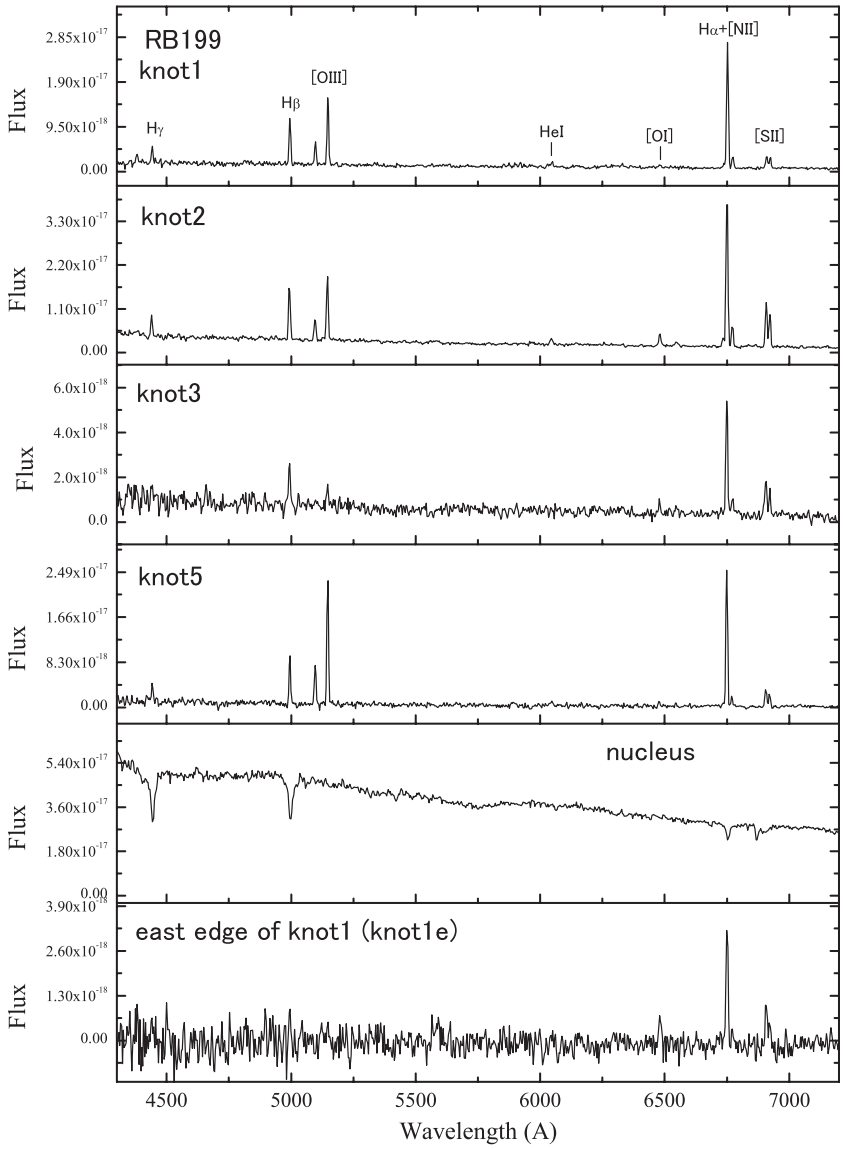

Figure 15. Spectra of the bright knots of the EIG and the nucleus of RB 199.

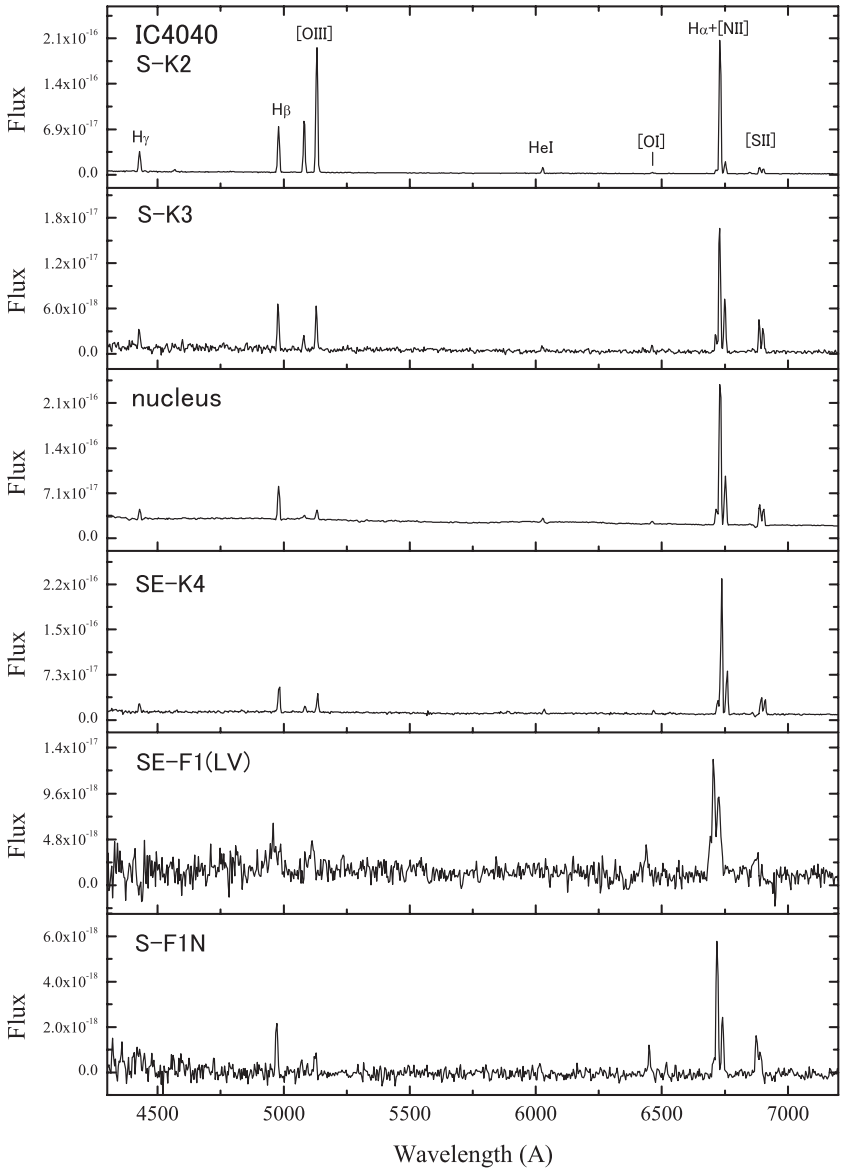

Figure 16. Spectra of the bright knots and filaments of the EIG and the nucleus of IC 4040.

the dusty gas flow in the disk of the galaxy (Figure 9), and S-K4 is embedded in the dusty flow.

Certain-low ionization forbidden lines, [S II], [O I], and [N II], are enhanced relative to Hα in some extended filaments of the IC 4040 EIG: SE-F1, S-F1, and S-F3 (Figure 16). An extended filament attached to the tip of knot 1 (east edge of knot 1) of RB 199 also exhibits enhanced [S II] and [O I], as shown in the bottom panel of Figure 15. Other extended filaments are too faint to measure the intensities of emission lines other than Hα.

Figures 18, 19, and 20 are emission-line diagnostic diagrams (Veilleux & Osterbrock 1987) of the EIG knots and filaments of RB 199 and IC 4040. These diagrams clearly show the above-mentioned characteristics of the EIG spectra. The relative weakness of [N II] λ6583 in the RB 199 EIG is conspicuous in Figure 18; the emission-line intensity ratio $\log([\mathrm{N\,II}]/\mathrm{H}\alpha) \leqslant -1.0$ for the knots of the RB 199 EIG. Extragalactic H II regions, which have low [N II]/Hα ratios, also generally have low [S II]/Hα and [O I]/Hα ratios. Figure 21 shows the abnormally weak [N II] emission of the RB 199 knots. The data points of knots 1e, 2, and 3 are well displaced from the main sequence of star-forming galaxies, whereas knots 1 and 5 are embedded in the sequence.

The emission-line ratios of the bright knots and the nucleus of IC 4040 with the exception of S-K2 are consistent with those of star-forming galaxies (Figures 18, 19, 20, and 21). Among these, it is clear that S-K2 of IC 4040 shows an emission-line spectrum like blue compact dwarf galaxies. In contrast, some extended filaments have LINER-like spectra. In particular, the [O I] line is enhanced in these features (Figure 20). This [O I] enhancement suggests that shock heating plays an important role in ionization and excitation of these features. The [N II] weak features in the RB 199 EIG also reveal similar [O I] enhancement, suggesting that shock heating is important for these peculiar features. However, the abnormally weak [N II] line of these features cannot be explained by ordinary shock-heating models. Low-velocity shock-heated gas that enhances [O I] and [S II] overlapped on low metal abundance H II regions might produce such peculiar emission-line intensity ratios.

We tried to estimate the metal abundance of the bright knots around RB 199 and IC 4040 using the model calculations

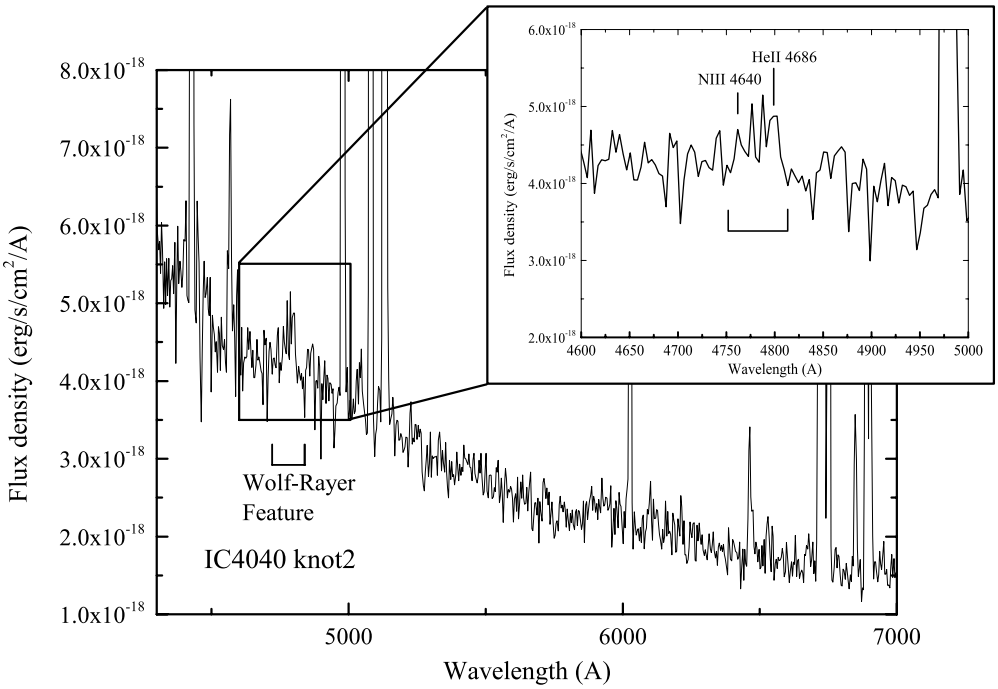

Figure 17. Expanded plot of the spectrum of S-K2 of the IC 4040 EIG. A broad bump at around 4650 Å (Wolf–Rayet feature) can clearly be seen (the significance of the detection is $\sim 3\sigma$). The insertion is an enlarged spectrum around the Wolf–Rayet feature. Although signal-to-noise ratio is not sufficiently high to allow us to decompose the feature into individual emission lines, He II λ4686 and N III λ4640 can be identified.

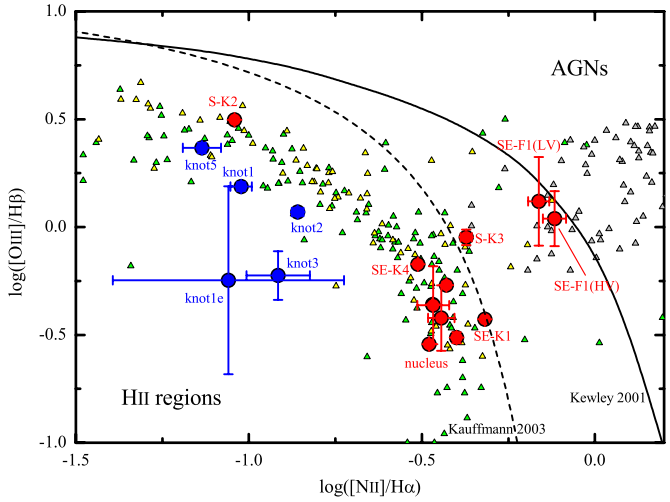

Figure 18. [O III] λ5007/Hβ ratio vs. [N II] λ6584/Hα ratio diagram. Blue circles represent the data points of the bright knots of the RB 199 EIG (see Figure 1). Red circles represent the data of the bright knots and filaments of the IC 4040 EIG (see Figure 2). The solid curve and dashed curve are demarcations between H II regions and active galactic nuclei (AGNs) proposed by Kewley et al. (2001) and Kauffmann et al. (2003), respectively. The green and yellow triangles are the data of H II regions of nearby field galaxies (Jansen et al. 2000) and the data of blue compact galaxies (Kong et al. 2002), respectively. The gray triangles are the data of LINERs (Ho et al. 1997).

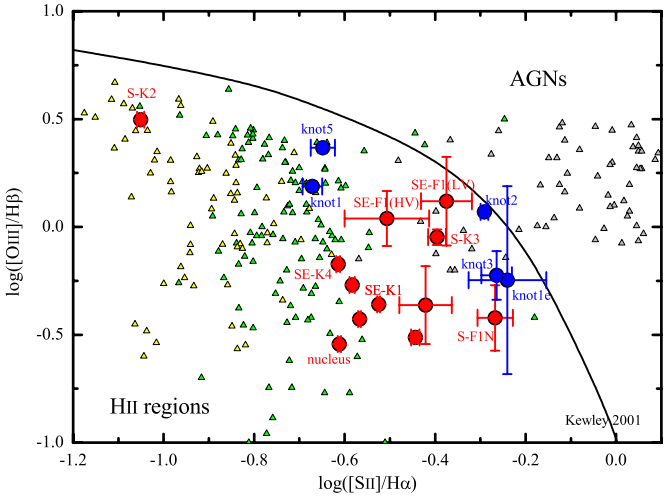

Figure 19. [O III] λ5007/Hβ ratio vs. [S II] λλ6716+6731/Hα ratio diagram. Symbols and curves are the same as in Figure 18.

by Kewley & Dopita (2002). We used [N II]/[O III] and [N II]/Hα ratios to estimate the metal abundance. The kinematical characteristics and oxygen abundances of the bright knots are shown in Table 3. The emission-line widths of most of the bright knots except for S-K2 are too narrow to resolve with our spectral resolution, indicating that the knots are much colder than the extended filaments. As suggested by the emission-line diagnostic diagrams (Figures 18, 19, and 20), the bright knots except for S-K3 and SE-K4 have basically low oxygen abundances: $\log(\mathrm{O/H}) + 12 \sim 8.4$–$8.6$. These values correspond to 0.5–0.8 $Z_\odot$. S-K3 of IC 4040 shows supersolar abundance ($\sim 1.6\ Z_\odot$). Because this knot is located at a marginal region between H II regions and LINERs in the diagnostic diagrams, shock heating may contribute enhancement of the forbidden lines, in particular, the [N II] line, of this knot.

4. DISCUSSION

4.1. Comparison with Ram Pressure Stripping Models

The one-sidedness of the morphologies of the EIGs of the Coma Cluster strongly suggests RPS as the primary formation mechanism of these features (YY08; YY10). All four of the observed EIGs exhibit a monotonically increasing pattern in their velocity fields. These types of velocity structures have

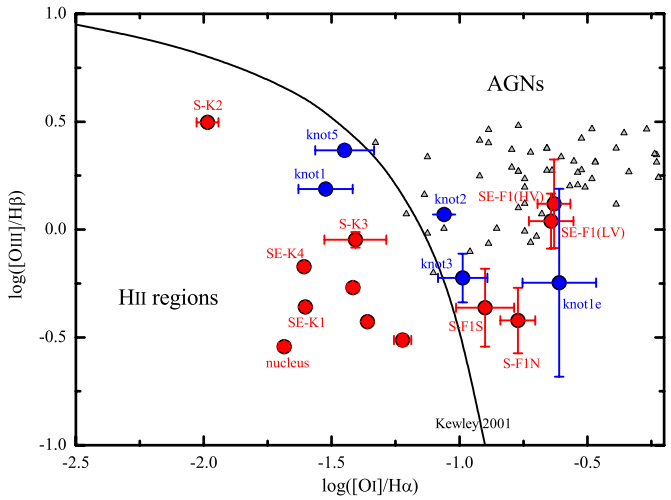

Figure 20. [O III] λ5007/Hβ ratio vs. [O I] λ6300/Hα ratio diagram. Symbols and curves are the same as in Figure 18.

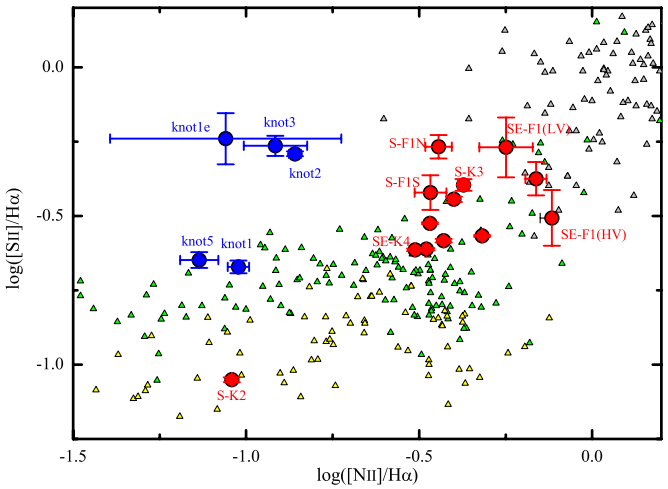

Figure 21. [N II] λ6583/Hα ratio vs. [S II] λλ6716+6731/Hα ratio diagram. Symbols are the same as in Figure 18.

Table 3
Kinematics and Abundances of the Bright Knots

ID	v_{rel} (km s^{-1})	σ[a] (km s^{-1})	log(O/H)+12	$Z_{\odot}$[b]
RB 199				
Knot 1	-104 ± 16	<70	8.38 ± 0.05	0.49 ± 0.08
Knot 2	-194 ± 15	<70	8.48 ± 0.05	0.62 ± 0.10
Knot 3	-210 ± 17	<70	8.40 ± 0.03	0.51 ± 0.07
Knot 5	-240 ± 15	<70	8.44 ± 0.05	0.56 ± 0.09
IC 4040				
S-K2	-241 ± 18	93 ± 20	8.59 ± 0.03	0.79 ± 0.10
S-K3	-268 ± 16	<70	8.88 ± 0.05	1.55 ± 0.25
SE-K4	-210 ± 17	<70	8.40 ± 0.02	0.51 ± 0.06

Notes.
[a] Velocity dispersion σ of Hα line derived by Gaussian fitting ($f(\lambda) \propto \exp(-\lambda^2/2\sigma^2)$).
[b] Oxygen abundances relative to the solar value derived by Asplund et al. (2009) (log(O/H) + 12 = 8.69 ± 0.05).

been suggested in many numerical simulations of RPS (Vollmer & Huchtmeier 2003; Roediger & Hensler 2005; Roediger & Brüggen 2008; Tonnesen & Bryan 2009, 2010).

Recently, Tonnesen & Bryan (2009, 2010) performed three-dimensional hydrodynamical simulations of RPS incorporating radiative cooling. They found that radiative cooling fragments the disk gas of ram-pressured galaxy. This fragmentation forms holes in the disk, and the holes accelerate the gas stripping. As a result, stripped gas flows straight behind the disk, such that the width of the wake of the stripped gas becomes much narrower than the width observed in models without cooling (Tonnesen & Bryan 2009). Tonnesen & Bryan (2010) examined observable values such as the density, velocity, and morphology of RPS wakes formed in simulations.

We compared the velocity fields of the EIGs around the Coma galaxies with those of the RPS simulations conducted by Tonnesen & Bryan (2010). Before making the comparison, we roughly estimated the age of the EIGs. The velocity gradient of the EIGs of RB 199 and IC 4040 is ∼7–10 km s^{-1} kpc^{-1}. The distances from the parent galaxies to the most distant filaments of the EIGs are ∼80–90 kpc. Assuming uniform acceleration with distance, a km s^{-1} kpc^{-1}, it takes $9.5 \times 10^2 \cdot \ln(d)/|a|$ Myr for the filaments to reach current locations, where d is the distance from the galaxy in units of kpc. In the case of the most distant filaments of RB 199 and IC 4040, it would thus be ∼700–900 Myr. Note that this number is the maximum value because the real flow is not a stationary accelerated one. The most distant part of the flow would be formed by the gas that was rapidly accelerated and reached its maximum speed in the early stage of the stripping event. Thus, the minimum age of the wake would be simply given by the length divided by the current velocity at the tip, ∼100 Myr. These values are consistent with those predicted for the 100 kpc scale wakes formed in RPS simulations (Abadi et al. 1999; Vollmer et al. 2001b; Schulz & Struck 2001; Roediger & Hensler 2005; Roediger et al. 2006; Jáchym et al. 2007; Roediger & Brüggen 2008; Tonnesen & Bryan 2010).

In the simulations conducted by Tonnesen & Bryan (2009, 2010), the velocity field of the stripped gas is highly turbulent in the early phase of RPS. Some gas components have very high velocities, close to the colliding velocity between the galaxy and the ICM, while some gas components have negative relative velocities with respect to the galaxy. After 250 Myr from the time of the galaxy–ICM collision, the velocity field morphology begins to smooth out. The relative velocity monotonically increases with the distance from the galaxy; the main part of the stripped gas has a relative velocity of 900 km s^{-1} at 150 kpc from the galaxy. The width of the velocity distribution is about 700 km s^{-1}. Figure 22 overlays the data points for IC 4040 on a velocity field map taken from Tonnesen & Bryan (2010). Clearly, the overall trend of the EIGs' velocity fields is consistent with the simulation. The acceleration rates of the stripped gas are 7–10 km s^{-1} kpc^{-1} for RB 199 and IC 4040, which is comparable to that of the main stream of the wake of the simulation: ≈6 km s^{-1} kpc^{-1}. Additionally, the simulation predicts that part of the stripped gas near the parent galaxy should have a very high relative velocity of ∼1000–1400 km s^{-1} (Figure 22). This feature corresponds to SE-F1 (LV) of IC 4040.

The main difference between the simulations and the observed data is the width of the velocity distribution. Numerical simulations made so far have predicted wide velocity distribution (∼1000 km s^{-1}) perpendicular to the stream direction. Tonnesen & Bryan (2010) predicted much narrower velocity distribution (700 km s^{-1}) by incorporating radiative cooling, but it is still larger than that seen in the observations. The velocity fields of the RB 199 and IC 4040 EIGs are well ordered except for SE-F1(LV). The width of the velocity distribution of

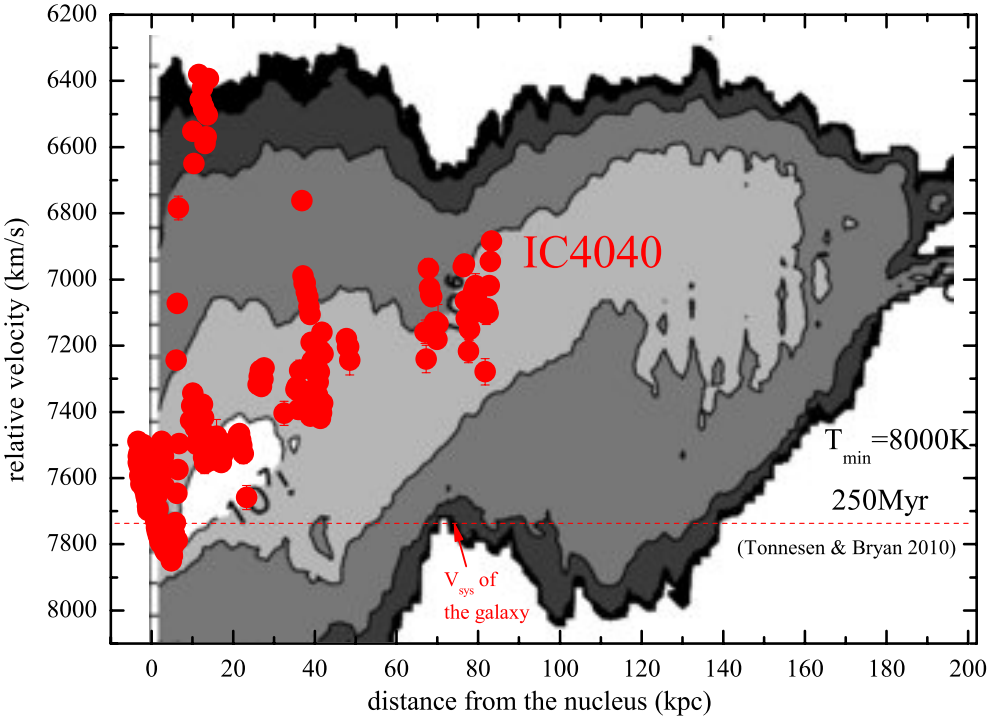

Figure 22. Velocity field of the EIG of IC 4040 (red circles) overlaid on that predicted by a numerical simulation made by Tonnesen & Bryan (2010). The observational data are not corrected for projection effects. The gray-scaled contours represent the velocity field of the stripped gas in the simulation at a time 250 Myr after the collision between the model galaxy and the ICM (Tonnesen & Bryan 2010, reproduced by permission of the AAS). The collision velocity is 1413 km s^{-1}. The cutoff temperature of the cooling curve of the model is $T_{\rm min} = 8000$ K.

(A color version of this figure is available in the online journal.)

the EIG of IC 4040 is about 300–400 km s^{-1}, which is a factor of two narrower than the simulations. This discrepancy may be partly due to insufficient spatial coverage and detection limit in our observations. We observed only the bright parts of the EIG filaments and could not follow the faint thin clouds, which may have much higher velocities than the bright dense clouds. Further, the spatial coverage of our observation was limited by slits. Thus, our observation did not cover the entire velocity field of the EIGs. A wide-field, two-dimensional spectroscopy would be needed for further quantitative comparison between observations and the simulations.

The morphology of the wake of the stripped gas also differed between the simulations and the observation. While many simulations predict a widely spread wake, most EIGs in the Coma Cluster have narrow, straight morphologies; the most remarkable example is the EIG around D100 (Yagi et al. 2007). The EIGs around GMP 2923 also have a narrow morphology. The EIGs around GMP 3071 and RB 199 are wider, but the widths do not exceed the size of the galaxies. Evaporation of an outer thin component of the stripped gas or some confinement mechanisms may narrow the morphology of the EIGs.

4.2. Star Formation in the EIG

Strong star formation activities can be seen in the bright knots in the EIGs of RB 199 and IC 4040. YY08 suggested, based on B, Hα, and *GALEX* UV images, that the bright knots in the EIG of RB 199 are star-forming regions. Smith et al. (2010) found asymmetric UV emission for 13 galaxies in the Coma center. They suggested that these emission regions were produced by active star formation in the stripped gas from their host galaxies. The sample of Smith et al. (2010) largely overlaps the EIG sample presented by YY10. Although YY10 did not identify optical continuum counterparts for most of the EIGs, Smith et al. (2010) pointed out that star formation activities are often associated with the EIGs (on the basis of their UV observations).

Recent numerical simulations of RPS have predicted active star formation in the stripped gas (Kronberger et al. 2008; Kapferer et al. 2008, 2009; Tonnesen & Bryan 2010; Tonnesen et al. 2011). YY08 reported good morphological agreement between the bright knots of the EIG of RB 199 and the numerical simulation of Kronberger et al. (2008) (see also Kapferer et al. 2009). Although the spatial resolution of these simulations is insufficient to reproduce molecular gas formation in the stripped gas, Yamagami & Fujita (2011) recently found that molecular clouds can be condensed in the RPS tails. They suggested that magnetic fields would play an important role in compressing the molecular clouds (Yamagami & Fujita 2011).

We compared the broadband colors of the star-forming knots of RB 199 (knot 1 to knot 5) and IC 4040 (S-K2) with a star formation model. Figure 23 is a $B - R_{\rm C}$ versus FUV $- B$ color–color plot for the star-forming knots. The loci of star formation model calculations using PEGASE.2 (Fioc & Rocca-Volmerange 1997) are also plotted in the figure. In these calculations, we assumed that stars are formed by infalling of gas. The infall rate was assumed to be proportional to $\exp(-t/t_i)/t_i$, where t_i is the infall timescale. We adopted $t_i = 100$ Myr. We also assumed that the initial mass function (IMF) follows the Salpeter IMF from 0.1 $M_\odot$ to 120 $M_\odot$, and the abundance of the infall gas is 0.6 $Z_\odot$. We did not include emission-line components in color calculation. Figure 23 presents two cases: an exponentially decaying star formation model with a decay timescale of 100 Myr, and a constant star formation model. YY08 showed similar plots for the RB 199 knots. However, we found that the filter transmission functions of the *GALEX* UV bands adopted by YY08 were incorrect, and the predicted FUV $- B$ colors were

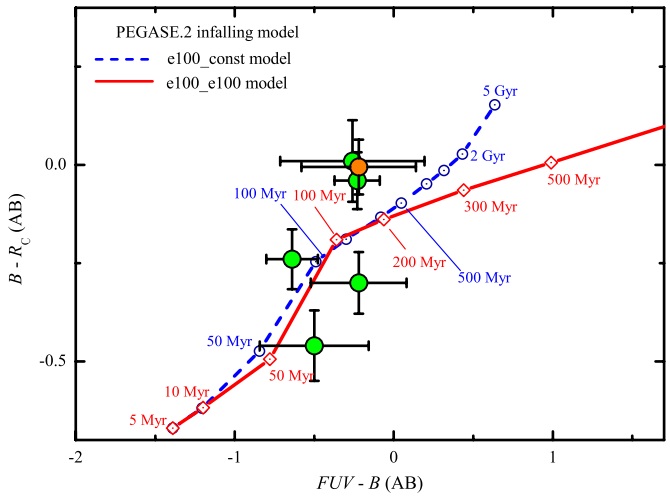

Figure 23. $B - R_C$ vs. FUV $- B$ color–color diagram of the bright knots of the EIG of RB 199 and IC 4040. Green points and orange points represent the data of the RB 199 knots and the IC 4040 knots, respectively. The red line and blue dashed line show loci of star formation models (using PEGASE.2, Fioc & Rocca-Volmerange 1997, see the text). Both models assume that stars are formed by infalling gas, and the infall rate is assumed to be proportional to $\exp(-t/t_i)/t_i$, where t_i is the timescale of the infall. We adopted $t_i = 100$ Myr. The red line is the result of an exponentially decaying star formation model with a decay timescale of 100 Myr. The blue dashed line is the result of a constant star formation model.

(A color version of this figure is available in the online journal.)

significantly shifted to the blue direction. Additionally, they did not subtract Hα emission contribution from the R_C band data. In this work, we used the correct *GALEX* FUV band transmission curve (Morrissey et al. 2005) to calculate the FUV magnitude of the models and the R_C magnitudes from which the Hα emission flux was carefully subtracted based on our spectroscopy.

Figure 23 shows that the star-forming knots are very young, on the order of 100 Myr. These bright knots are located at ∼20 kpc from the parent galaxies with a current relative velocity of ∼200 km s^{-1}. Thus, it would take at least ∼100 Myr for these knots to reach the current positions. This is comparable to or slightly shorter than the age estimation for the knots. However, the real travel time of the knots would be a few times longer than this value because the knots are currently accelerated. Together with the low metal abundance nature of the knots (see Section 3.2), this thus suggests that the majority of the stellar component of these knots was formed in the stripped metal-poor gas that originally resided in the outskirts of the parent galaxies. Current active star formation associated with the knots also supports this idea. Using hybrid *N*-body/hydrodynamical simulations, Kapferer et al. (2009) found that 95% of stars newly formed by RPS reside in the wake of stripped gas. In their simulations, the timescale of star formation in the wakes is ∼100 Myr (Kapferer et al. 2009). The young age of the star-forming knots of the EIGs suggested by our results is consistent with their findings.

4.3. Overlapped Ionized Gas in the EIG of RB 199

We found that an ionized gas cloud overlaps the line of sight to Hα cloud 2 of RB 199. This cloud has a radial velocity of 6500 km s^{-1}, which is much slower than that of the EIG (∼8000 km s^{-1}) and closer to the mean velocity of the Coma Cluster. It indicates that this overlapped cloud is kinematically independent with the EIG.

What is this cloud and where did it originate? One possibility is that it is a gas cloud stripped from a nearby galaxy. A candidate of the parent galaxy is an early-type galaxy (SDSS J125844.32+274251.6) near Hα cloud 2. According to the SDSS database,[6] the color of this galaxy is typical of S0 galaxies. Unfortunately, the recession velocity of this galaxy is not known. No morphological indication suggests a physical connection between this galaxy and the overlapped cloud. We thus concluded that this galaxy is plausibly not the parent of the cloud.

On the other hand, this cloud may be a remnant of a stripping event that occurred long ago. In this case, identifying the parent galaxy would be difficult because an apparent physical connection between them would be almost completely lost.

Recently, a huge intracluster stellar population has been found in local- and intermediate-redshift clusters (Gregg & West 1998; Gonzalez et al. 2000; Mihos et al. 2005; Krick & Bernstein 2007). Such a population is thought to be originated by galaxy–galaxy interaction or merger in the central region of the clusters. Tidal force associated with galaxy–galaxy interaction would strip the stars from the galaxies and spread them into the intracluster space. Associated with these tidal stripping events, dense disk gas may be also stripped, and a dense gas cloud may be floating in the intracluster space.

Although it is impossible to reach any conclusions from this rare example, this finding may suggest that there is a population of "floating ionized gas" in clusters of galaxies (Gerhard et al. 2002; Cortese et al. 2004). Deep Hα imaging of intracluster space and spectroscopic follow-up will reveal how common these kinds of objects are in galaxy clusters.

4.4. Fate of the EIG

Our spectroscopic observations showed that it is plausible that the EIGs associated with the four galaxies RB 199, IC 4040, GMP 2923, and GMP 3071 are formed by RPS. The observations also made it clear that strong star formation occurs in some parts of the stripped gas.

The EIGs around galaxies in the Coma Cluster may act as a snapshot of a formation process of a very faint galaxy population in clusters. The typical brightness and size of the bright knots in the EIGs are $M_R \sim -12$ to -13 and 1–2 kpc (corresponding half-light radius ≈200–300 pc), respectively, which are similar to those of ultracompact dwarf galaxies (Drinkwater et al. 2004) or small dwarf spheroidals. This suggests that the bright knots are gravitationally self-bound systems.[7] In this case, they would survive and float in the halo of the parent galaxies or in the intracluster space of the Coma. After the star formation ceases, the luminosities of the bright knots will significantly decrease. Assuming the exponentially decaying star formation model we used in Section 4.2, and assuming that a typical age for the bright knots is 200 Myr, we can conclude that the luminosities of the knots would decrease by 2–3 mag in *R* band in 1 Gyr. That is, the absolute magnitudes of the knots will eventually be $M_R \sim -10$ to -11. This luminosity range is within that of the dwarf spheroidal galaxies in the local group (Belokurov et al. 2007).

Most of the stars of the EIGs may be bound to the gravitational field of the parent galaxies. Kronberger et al. (2008) discussed

[6] http://www.mpa-garching.mpg.de/SDSS/DR7/

[7] Of course, measuring stellar velocity dispersion of the knots is necessary to check whether they are really self-bound systems or not, but the spectral resolution and coverage of our spectroscopic data are not enough to perform such a study.

that most of the stars formed in the stripped gas in their simulations are gravitationally bound to the host galaxy and will fall back to the galaxy within 1 Gyr. In this case, the bright knots may be observed as features like "galaxy aggregates" identified in the Coma Cluster by Conselice & Gallagher (1998) in the fall-back process. Because stellar systems are collisionless ones, the stars will penetrate the galaxy disk and oscillate between two sides of the disk. Accordingly, the bright knots and the blue filaments will eventually be destroyed and distributed widely in the galaxy halo; in other words, the knots would form the halo population of the galaxy.

However, our spectroscopy revealed that the ionized gas of the knots has a relative velocity of 200–270 km s^{-1} (Table 3). Because the stellar components of the knots are closely associated with the ionized gas, the stars would have almost the same velocity as the ionized gas. In this case, the knots probably escape from the gravitational potential of the parent galaxies and float into the intracluster space. In this context, it is interesting to note that an intracluster H II region was found in the Virgo Cluster (Gerhard et al. 2002; Okamura et al. 2002).

5. SUMMARY

We have presented the results of deep imaging and spectroscopic observations of very EIG around four member galaxies of the Coma Cluster, RB 199, IC 4040, GMP 2923, and GMP 3071. Among them, the bright EIG around IC 4040 is remarkable and has complex morphology. It consists of two streams extending toward the southeast and southern directions from the galaxy. The southeast stream is connected to the central active star formation region. Many small ionized clouds are distributed between the southern stream and IC 4040. Several star-forming blue knots are embedded in the EIGs of RB 199 and IC 4040. The extension of the EIGs ranges from ∼35 kpc to ∼80 kpc.

The relative radial velocities of the EIGs with respect to the systemic velocity of the parent galaxies from which they emanate increase almost monotonically with the distance from the nucleus of the respective galaxies, reaching ∼−400 to −800 km s^{-1} at around 40–80 kpc from the galaxies. The velocity decreasing rates are −7 to − 10 km s^{-1} kpc^{-1} for RB 199, IC 4040, and GMP 2923. The GMP 3079 EIG has the steepest velocity gradient of −25 km s^{-1} kpc^{-1}. The kinematics of the EIGs is consistent with the concept that high-speed collisions between the ICM and infalling galaxies of the Coma Cluster form these features because all the sample galaxies have systemic velocities much higher than the mean recession velocity of the cluster. We obtained a detailed velocity field for the bright EIG of IC 4040. The velocity dispersions of the diffuse filaments of the IC 4040 EIG reach ∼200–400 km s^{-1}. We also found a very low velocity filament at the southeastern edge of the disk of IC 4040. The filament has a velocity of −1300 km s^{-1} relative to the systemic velocity of the galaxy.

Some of the bright compact knots in the EIGs of RB 199 and IC 4040 have blue continuum and strong Hα emission. The equivalent widths of the Hα emission of the knots range 200–1500 Å. The emission-line intensity ratios of the knots are basically consistent with those of sub-solar abundance H II regions. These facts indicate that intensive star formation occurs in the knots. Some filaments, including the low-velocity filament of the IC 4040 EIG, exhibit shock-like emission-line spectra, suggesting that shock heating plays an important role in ionization and excitation of the EIGs.

The morphologies and velocity fields of the EIGs are broadly consistent with those predicted by numerical simulations of RPS. Our spectroscopic observations did not cover the entire regions of the EIGs due to spatial limitation of slits. This prevented us from making detailed comparison between the observation and the simulations. Deep and wide integral field spectroscopy would allow us to compare the kinematics of the EIGs with the prediction of numerical simulations in detail.

We are grateful to the staff of the Subaru telescope for their kind help with the observations. We thank the anonymous referee for valuable comments that significantly improve this paper. This work was in part carried out using the data obtained by a collaborative study on the Coma Cluster. This study was in part carried out using the facilities at the Astronomical Data Analysis Center (ADAC), National Astronomical Observatory of Japan. This research made use of NASA's Astrophysics Data System Abstract Service, NASA/IPAC Extragalactic Database, SDSS skyserver, and *GALEX* GR5 database. This work was financially supported in part by Grant-in-Aid for Scientific Research No. 23244030 from the Japan Society for the Promotion of Science (JSPS) and No. 19047003 from the Ministry of Education, Culture, Sports, Science and Technology (MEXT).

REFERENCES

Abadi, M. G., Moore, B., & Bower, R. G. 1999, MNRAS, 308, 947
Abramson, A., Kenney, J. D. P., Crowl, H. H., et al. 2011, AJ, 141, 164
Asplund, M., Grevesse, N., Sauval, A. J., & Scott, P. 2009, ARA&A, 47, 481
Bekki, K., & Couch, W. J. 2003, ApJ, 596, L13
Belokurov, V., Zucker, D. B., Evans, N. W., et al. 2007, ApJ, 654, 897
Boselli, A., Boissier, S., Cortese, L., & Gavazzi, G. 2008, ApJ, 674, 742
Boselli, A., & Gavazzi, G. 2006, PASP, 118, 517
Bravo-Alfaro, H., Cayatte, V., van Gorkom, J. H., & Balkowski, C. 2000, AJ, 119, 580
Bravo-Alfaro, H., Cayatte, V., van Gorkom, J. H., & Balkowski, C. 2001, A&A, 379, 347
Butcher, H., & Oemler, A. 1978, ApJ, 219, 18
Butcher, H., & Oemler, A. 1984, ApJ, 285, 426
Byrd, G., & Valtonen, M. 1990, ApJ, 350, 89
Cayatte, V., Kotanyi, C., Balkowski, C., & van Gorkom, J. H. 1994, AJ, 107, 1003
Cayatte, V., van Gorkom, J. H., Balkowski, C., & Kotanyi, C. 1990, AJ, 100, 604
Chemin, L., Cayatte, V., Balkowski, C., et al. 2005, A&A, 436, 469
Chung, A., van Gorkom, J. H., Kenney, J. D. P., Crowl, H., & Vollmer, B. 2009, AJ, 138, 1741
Chung, A., van Gorkom, J. H., Kenney, J. D. P., & Vollmer, B. 2007, ApJ, 659, L115
Conselice, C. J., & Gallagher, J. S. 1998, MNRAS, 297, L34
Cortese, L., Catinella, B., Boissier, S., Boselli, A., & Heinis, S. 2011, MNRAS, 415, 1797
Cortese, L., Davies, J. I., Pohlen, M., et al. 2010, A&A, 518, L49
Cortese, L., Gavazzi, G., Boselli, A., & Iglesias-Paramo, J. 2004, A&A, 416, 119
Cortese, L., Gavazzi, G., Boselli, A., et al. 2006, A&A, 453, 847
Cortese, L., Marcillac, D., Richard, J., et al. 2007, MNRAS, 376, 157
Crowl, H. H., Kenney, J. D. P., van Gorkom, J. H., & Vollmer, B. 2005, AJ, 130, 65
Dressler, A. 1980, ApJ, 236, 351
Dressler, A. 1994, ApJ, 430, 107
Drinkwater, M. J., Gregg, M. D., Couch, W. J., et al. 2004, PASA, 21, 375
Fioc, M., & Rocca-Volmerange, B. 1997, A&A, 326, 950
Fujita, Y. 2004, PASJ, 56, 29
Fujita, Y., & Nagashima, M. 1999, ApJ, 516, 619
Fumagalli, M., Gavazzi, G., Scaramella, R., & Franzetti, P. 2011, A&A, 528, A46
Gavazzi, G., Boselli, A., Mayer, L., et al. 2001, ApJ, 563, L23
Gavazzi, G., Cortese, L., Boselli, A., et al. 2003, ApJ, 597, 210
Gerhard, O., Arnaboldi, M., Freeman, K. C., & Okamura, S. 2002, ApJ, 580, L121
Gonzalez, A. H., Zabludoff, A. I., & Zaritsky, D. 2000, ApJ, 618, 195
Gregg, M. D., & West, M. J. 1998, Nature, 396, 549
Gunn, J. E., & Gott, J. R. 1972, ApJ, 176, 1

Henriksen, M., & Byrd, G. 1996, ApJ, 459, 89
Hester, J. A., Seibert, M., Neill, J. D., et al. 2010, ApJ, 716, L14
Ho, L. C., Filippenko, A. V., & Sargent, W. L. W. 1997, ApJS, 112, 391
Jáchym, P., Palouš, J., Köppen, J., & Combes, F. 2007, A&A, 472, 5
Jansen, R. A., Fabricant, D., Franx, M., & Caldwell, N. 2000, ApJS, 126, 331
Kapferer, W., Kronberger, T., Ferrari, C., Riser, T., & Schindler, S. 2008, MNRAS, 389, 1405
Kapferer, W., Sluka, C., Schindler, S., Ferrari, C., & Ziegler, B. 2009, A&A, 499, 87
Kashikawa, N., Aoki, K., Asai, R., et al. 2002, PASJ, 54, 819
Kauffmann, G., Heckman, T. M., Tremonti, C., et al. 2003, MNRAS, 346, 1055
Kenney, J. D. P., & Koopmann, R. A. 1999, AJ, 117, 181
Kenney, J. D. P., Tal, T., Crowl, H. H., Feldmeier, J., & Jacoby, G. H. 2008, ApJ, 687, L69
Kennicutt, R. C. 1998, ApJ, 498, 541
Kewley, L. J., & Dopita, M. A. 2002, ApJS, 142, 35
Kewley, L. J., Dopita, M. A., Sutherland, R. S., Heisler, C. A., & Trevena, J. 2001, ApJ, 556, 121
Kong, X., Cheng, F. Z., Weiss, A., & Charlot, S. 2002, A&A, 396, 503
Koopmann, R., & Kenney, J. D. P. 2004, ApJ, 613, 866
Krick, J. E., & Bernstein, R. A. 2006, AJ, 134, 466
Kronberger, T., Kapferer, W., Ferrari, C., Unterguggenberger, S., & Schindler, S. 2008, A&A, 481, 337
Mihos, J. C., Harding, P., Feldmeier, J., & Morrison, H. 2005, ApJ, 631, L41
Miyazaki, S., Komiyama, Y., Sekiguchi, M., et al. 2002, PASJ, 54, 833
Moore, B., Katz, N., Lake, G., Dressler, A., & Oemler, A. 1996, Nature, 379, 613
Morrissey, P., Schiminovich, D., Barlow, T. A., et al. 2005, ApJ, 619, L7
Okamoto, T., & Nagashima, M. 2003, ApJ, 587, 500
Okamura, S., Yasuda, N., Arnaboldi, M., et al. 2002, PASJ, 54, 883
Oosterloo, T., & van Gorkom, J. 2005, A&A, 437, L19
Poggianti, B. M., Bridges, T. J., Komiyama, Y., et al. 2004, ApJ, 601, 197
Postman, M., & Geller, M. J. 1984, ApJ, 281, 95
Randall, S., Nulsen, P., Forman, W. R., et al. 2008, ApJ, 688, 208
Roediger, E., & Brüggen, M. 2008, MNRAS, 388, 465
Roediger, E., Brüggen, M., & Hoeft, M. 2006, MNRAS, 371, 609
Roediger, E., & Hensler, G. 2005, A&A, 433, 875
Sakai, S., Kennicutt, R. C., Jr., van der Hulst, J. M., & Moss, C. 2002, ApJ, 578, 842
Schulz, S., & Struck, C. 2001, MNRAS, 328, 185
Sivanandam, S., Rieke, M. J., & Rieke, G. H. 2010, ApJ, 717, 147
Smith, R. J., Lucey, J. R., Hammer, D., et al. 2010, MNRAS, 408, 1417
Solanes, J. M., Manrique, A., García-Gómez, C., et al. 2001, ApJ, 548, 97
Sun, M., Donahue, M., Roediger, E., et al. 2010, ApJ, 708, 946
Sun, M., Donahue, M., & Voit, M. 2007, ApJ, 671, 170
Tonnesen, S., & Bryan, G. L. 2009, ApJ, 694, 789
Tonnesen, S., & Bryan, G. L. 2010, ApJ, 709, 1203
Tonnesen, S., Bryan, G. L., & Chen, R. 2011, ApJ, 731, 98
van der Wel, A., Bell, E. F., Holden, B. P., Skibba, R. A., & Rix, H.-W. 2010, ApJ, 714, 1779
van der Wel, A., Holden, B. P., Franx, M., et al. 2007, ApJ, 670, 206
van Gorkom, J. H. 2004, in Clusters of Galaxies: Probes of Cosmological Structure and Galaxy Evolution, ed. J. S. Mulchaey, A. Dressler, & A. Oemler (Cambridge: Cambridge Univ. Press), 305
Veilleux, S., & Osterbrock, D. M. 1987, ApJS, 63, 295
Vollmer, B. 2009, A&A, 502, 427
Vollmer, B., Braine, J., Balkowski, C., Cayatte, V., & Duschl, W. J. 2001a, A&A, 374, 824
Vollmer, B., Brane, J., Pappalardo, C., & Hily-Blant, P. 2008, A&A, 491, 445
Vollmer, B., Cayatte, V., Balkowski, C., & Duschl, W. J. 2001b, ApJ, 561, 708
Vollmer, B., & Huchtmeier, W. 2003, A&A, 406, 427
Vollmer, B., Soida, M., Chung, A., et al. 2009, A&A, 496, 669
Yagi, M., Komiyama, Y., Yoshida, M., et al. 2007, ApJ, 660, 1209
Yagi, M., Yoshida, M., Komiyama, Y., et al. 2010, AJ, 140, 1814 (YY10)
Yamagami, T., & Fujita, Y. 2011, PASJ, 63, 1165
Yoshida, M., Ohyama, Y., Iye, M., et al. 2004, AJ, 127, 90
Yoshida, M., Yagi, M., Komiyama, Y., et al. 2008, ApJ, 688, 918 (YY08)
Yoshida, M., Yagi, M., Okamura, S., et al. 2002, ApJ, 567, 118